Channel cross-section heterogeneity of particulate organic carbon transport in the Huanghe

Yutian Ke[1][†], Damien Calmels[1], Julien Bouchez[2], Marc Massault[1], Benjamin Chetelat[3], Aurélie Noret[1], Hongming Cai[2], Jiubin Chen[3], Jérôme Gaillardet[2], Cécile Quantin[1]

[1]GEOPS, Université Paris-Saclay-CNRS, 91405 Orsay, France
[2]Université de Paris, Institut de Physique du Globe de Paris, CNRS, 75005 Paris, France
[3]School of Earth System Science, Institute of Surface-Earth System Science, Tianjin University, 300072 Tianjin, China
[†]Present address: Division of Geological and Planetary Science, California Institute of Technology, Pasadena, CA 91125, USA

Corresponding author: Yutian KE (yutianke@caltech.edu)

Abstract. The Huanghe (Yellow River), one of the largest turbid river systems in the world, has long been recognized as a major contributor of suspended particulate matter (SPM) to the ocean. However, over the last few decades, the SPM export flux of the Huanghe has decreased over 90% due to the high management, impacting the global export of particulate organic carbon (POC). To better constrain sources and modes of transport of POC beyond the previously investigated transportation of POC near the channel surface, SPM samples were for the first time collected over a whole channel cross-section in the lower Huanghe. Riverine SPM samples were analyzed for particle size and major element contents, as well as for POC content and dual carbon isotopes (^{13}C and ^{14}C). Clear vertical and lateral heterogeneities of the physical and chemical properties of SPM are observed within the river cross-section. For instance, finer SPM carry in general more POC with higher ^{14}C activity near the surface of the right bank. Notably, we discuss how bank erosion in the alluvial plain is likely to generate lateral heterogeneity in POC composition. The Huanghe POC is millennial-aged (4,020 ± 500 radiocarbon years), dominated by organic carbon (OC) from the biosphere, while the lithospheric fraction reaches up to ca. 33%. The mobilization of aged and refractory OC, including radiocarbon-dead biospheric OC, from deeper soil horizons of the loess-paleosol sequence through erosion in the Chinese Loess Plateau is an important mechanism contributing to fluvial POC in the Huanghe drainage basin. Altogether, anthropogenic activities can drastically change the compositions and transport dynamics of fluvial POC, consequentially altering the feedback of the source-to-sink trajectory of a river system to regional and global carbon cycles.

1 Introduction

Rivers are the main conveyor of rock and soil debris eroded from the continents to the ocean. Along with inorganic material, river sediments host particulate organic carbon (POC) derived mainly from three major sources: 1) recently photosynthesized OC of the biosphere, 2) aged and altered OC from soils, and 3) ancient OC contained in sedimentary rocks (Blair et al., 2010). The net effect of riverine POC transport on the carbon cycle and thus on the evolution of Earth's climate depends on POC provenance and fate. The effective sedimentary burial of POC derived from the terrestrial biosphere (biospheric OC, OC_{bio}) represents a net, long-term sink of atmospheric CO_2 (Galy et al., 2007, Bouchez et al., 2014; Hilton et al., 2015), whereas the oxidation of POC derived from continental rocks (petrogenic OC, OC_{petro}) acts as a net, long-term source of CO_2 to the atmosphere (Hilton et al., 2014). The erosion and burial of OC_{petro} escaping from oxidation has no net effect on the long-term carbon cycle (Galy et al., 2008a; Bouchez et al., 2010; Hilton et al., 2011; Horan et al., 2019). In addition, the reactive nature of OC_{bio} might also result in short-term CO_2 emission during transport from both river channels and recently-deposited sediments (Mayorga et al., 2005; Galy and Eglinton, 2011; Blair and Aller, 2012).

Globally, rivers transport a total POC flux of *ca.* 200 Tg C/year, consisting of 157^{+74}_{-50} Tg C/year of OC_{bio} and 43^{+61}_{-25} Tg C/year of OC_{petro} (Galy et al., 2015; Ludwig et al., 1996). Source-to-sink processes controlling the origin and fate of riverine POC are prominently river-specific, suggesting that the impact of POC on regional and global carbon cycles might significantly vary both spatially and temporally (Blair and Aller, 2012). It is thus crucial to understand the mechanisms controlling the POC export by large rivers that integrate vast portions of the land surface, and quantify the differing sources of carbon exported by those large river systems.

The Huanghe (Yellow River) is a highly turbid river system that exports over 85% of its OC as particulate matter, with efficient deposition and preservation in the ocean (Cauwet and Mackenzie, 1993; Bianchi, 2011; Zhang et al., 2013; Ran et al., 2013). The Huanghe has been highly managed over the last few decades through water and soil conservation measures as well as reservoir construction, leading to a decrease of nearly 90% of its sediment load (Wang and Fu et al., 2016; Wang et al., 2007; Milliman et al., 1987) and a significant decrease in its POC delivery to the ocean (Zhang et al., 2013). Reservoir construction dramatically affects the transport and fate of both sediment load and POC in large rivers (Syvitski et al., 2005; Li et al., 2015). The estimated POC flux of the Huanghe is thought to have shifted from 4.5 Tg C/yr in the 1980s (Cauwet and Mackenzie, 1993) to 0.34-0.58 Tg C/yr nowadays (Tao et al., 2018) in response to both anthropogenic influence (Hu et al., 2015; Tao et al., 2018; Yu et al., 2019a) and natural variability of the regional hydrological cycle (Qu et al., 2020). These large-scale perturbations have likely modified the OC input from the different terrestrial pools as well as the fate of exported POC that was previously reaching deposition centers in the ocean and that now remains stuck on land. Those alterations of the carbon cycle remain to be addressed.

Over the last decade, POC transport in the Huanghe has been investigated for 1) determination and quantification of POC sources, based on bulk or molecular carbon isotopic composition (Tao et al., 2015; Yu et al., 2019b; Ge et al., 2020; Qu et al., 2020); 2) temporal and spatial variations in POC export and distribution among different size fractions (Ran et al., 2013; Wang 2012; 2016; Yu et al., 2019a, b ; Qu et al., 2020); 3) impact of anthropogenic activities (Hu

65   et al., 2015; Tao et al., 2018; Yu et al., 2019a); and 4) burial efficiency and preservation in the ocean (Sun et al., 2018;

66   Tao et al., 2016; Ge et al., 2020). However, all these previous studies rely on suspended sediment samples collected

67   near the channel surface or at a single, intermediate depth in the river channel, further assuming a homogeneous

68   distribution of suspended sediment characteristics in the water column, both vertically and laterally. It is now well

69   recognized that suspended sediments present physical, mineralogical, chemical, and isotopic heterogeneities across

70   river transect due to hydrodynamic sorting and tributary mixing (Galy et al., 2008b; Garzanti et al., 2010; Bouchez et

71   al., 2010, 2011a). This is also true for POC, whose age and composition vary following vertical water depth (*e.g.,*

72   Galy et al., 2008b; Bouchez et al., 2014; Hilton et al., 2015; Repasch et al., 2021; Schwab et al., 2022), and lateral

73   river transect (*e.g.*, Bouchez et al., 2014; Baronas et al., 2020), and between sediment size fractions separated in the

74   laboratory (Yu et al., 2019b; Ge et al., 2020). Such heterogeneity warrants a re-evaluation of POC transport in the

75   Huanghe, accounting for the variability in suspended sediment characteristics over the channel cross-section.

76   In this study, we take advantage of in-river hydrodynamic sorting to access the full range of suspended sediment size

77   fractions by collecting suspended particulate matter (SPM) samples along several river depth profiles distributed

78   across a channel transect (*e.g.*, Bouchez et al., 2014; Freymond et al., 2018; Baronas et al., 2020). We apply this

79   sampling scheme to a cross-section of the Huanghe located 200 km upstream from the river mouth and report SPM

80   OC content, stable isotope composition, and radiocarbon activity as well as total nitrogen, major element composition

81   (aluminum and silicon), and particle size distribution. Based on these novel samples and data sets, this study aims at

82   1) determining the controls on POC content in the Huanghe; 2) tracing and quantifying the sources of riverine POC

83   in the Huanghe; and 3) providing depth-integrated estimates of POC fluxes in the most turbid large river system.

84   **2 Study area**

85   The Huanghe originates from the north-eastern Qinghai-Tibet Plateau (QTP) and runs through the Chinese Loess

86   Plateau (CLP) and the North China Plain (NCP) to the Bohai Sea (Figure 1a). It is 5,464 km long and drains a basin

87   area of 79.5×10^4 km². The Huanghe drainage basin can be subdivided into three main geomorphic units: 1) the high-

88   relief upper reaches spanning from the source region (elevation of 4,500 m) to the city of Toudaoguai (located 3,472

89   km downstream at an elevation of 1,000 m); 2) the middle reaches with a channel length of 1,206 km, ending at

90   Huayuankou (elevation of 110 m) draining landscapes characterized by relatively gentle slopes; and 3) the lower

91   reaches where the river flows eastwards across a fluvial plain over a length of 786 km. These three sections drain

92   53.8%, 43.3%, and 2.9% of the whole Huanghe basin area, respectively (Wang et al., 2007; YRCC, 2016). Most

93   second-order tributaries drain the CLP region and feed the main channel in the middle reaches, the Dawenhe River

94   being the only tributary of the lower reaches, with negligible water and sediment supply due to upstream trapping in

95   lakes and reservoirs. It is worth noting that more than 50% of the water discharge at the Huanghe's mouth comes from

96   the QTP, whereas over 90% of the sediment load originates from the CLP (Wang et al., 2010, 2017; Pan et al., 2016).

97   The CLP is thus the principal source area of sediment to the Huanghe (Shi and Shao, 2000; Guo et al., 2002; Wang

98   and Fu et al., 2016).

99   The Huanghe drainage basin is mostly underlain by the North China craton, and is bounded by several mountain belts.

100   The watershed encompasses 46% of sedimentary rock outcrops (mainly siliciclastic rocks with minor carbonates), and

101 about 45% of unconsolidated sediments (mainly Quaternary loess deposits). The remaining outcrops include
102 metamorphic, plutonic, and volcanic rocks formed from the Archean to the Tertiary (Figure S1). Although river
103 incision is strong in the QTP, a substantial part of the corresponding eroded material is not effectively transferred to
104 the lower reaches due to deposition in the CLP and the western Mu-Us desert, a situation that has prevailed since at
105 least the middle Pleistocene (Nie et al., 2015; Licht et al., 2016; Pan et al., 2016). In addition, recent anthropogenic
106 disturbance such as constructions of large dams in the upper reaches has profoundly modified the export of solid
107 materials from the basin (Wang et al., 2007). The Huanghe then flows through the CLP that has acted as the major
108 supplier of sediment to the system since at least the Calabrian Pleistocene (Stevens et al., 2013; Bird et al., 2015).
109 There, an easily erodible loess-paleosol formation has accumulated since 2.58 Ma (Guo et al., 2002), over a thickness
110 ranging from a few meters to more than 500 m, with an average of 100 m. This loess-paleosol formation and underlying
111 Cretaceous sedimentary rocks are actively incised by the main stem and its tributaries (Shi and Shao, 2000; Guo et
112 al., 2002; Wang and Fu et al., 2016). Notably, the Ordos Basin underlying the CLP is rich in oil and gas (Guo et al.,
113 2014). In the lower reaches, the river drains Quaternary fluvial deposits and sedimentary rocks.

114 The Huanghe drainage basin encompasses the entire arid and semi-arid region of northern China in the upper and
115 middle reaches, and is characterized by more humid climate conditions in the lower reaches. Annual average
116 precipitation (over the period 1950 - 2000) in the upper, middle and lower reaches regions is 368 mm, 530 mm, and
117 670 mm, respectively (Wang et al., 2007). As a result of the East Asian summer and winter monsoon circulations, the
118 rainy season (June to September) contributes 85% of the annual precipitation (Wang et al., 2007). During the rainy
119 season, frequent storm events lead to concentrated flows (relatively high discharge) in vulnerable gully-hill systems,
120 the dominant regional geomorphic landscape, and actively participates in soil erosion in the CLP (Shi and Shao, 2000;
121 He et al., 2004; Qu et al., 2020). The present-day (2002 to 2016) suspended sediment flux delivered by the Huanghe
122 to the sea is about 0.12 Gt/yr, which implies a decrease of nearly 90% in sediment export compared to the widely cited
123 estimate of 1.08 Gt/yr (average value between 1950 to 1980, Milliman and Farnsworth, 2011). This massive decrease
124 in sediment export mostly results from human perturbations, including soil conservation practices in the CLP and
125 retention in large reservoirs, rather than from climatic variations such as the decreasing precipitation observed in the
126 region over the last decades (Wang et al., 2007; Ran et al., 2013; Wang and Fu et al., 2016; Li et al., 2022). A scheme
127 for water and sediment regulation (WSR) has been implemented through the construction of the Xiaolangdi Reservoir
128 since 2002, aiming to mitigate water and sediment imbalances in the lower reaches. This regulation has resulted in a
129 modification of the flux of sediment delivered to the lower reaches and estuary, making the Huanghe a highly human-
130 regulated river system. However, no WSR was implemented in 2016, the year of our sampling campaign, suggesting
131 that the collected SPM samples are not significantly affected by retention in dams, and thus are representative of the
132 fluvial transport of terrestrial materials eroded from the CLP.
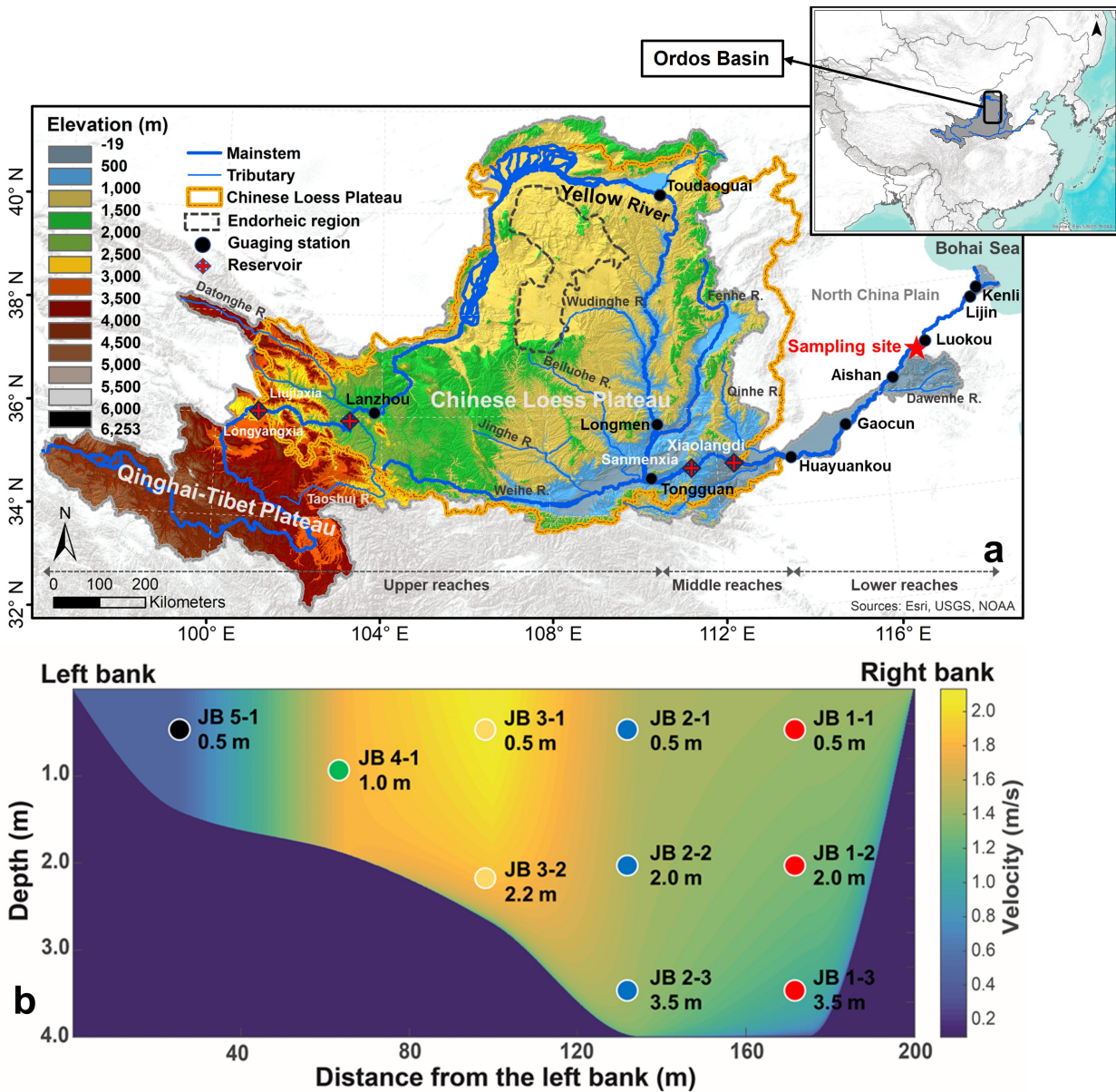
Figure 1: (a) Elevation map of the Huanghe drainage basin showing the main reservoirs and gauging stations along the main stem as well as our sampling site (36.75ºN, 117.02ºE, near the Luokou gauging station); and (b) channel cross-section sampled for this study showing the depth and lateral distribution of suspended particulate matter (SPM) samples and modeled velocity distribution based on the "law of the wall", using the point velocity data measured by a current velocity meter attached to the sampler.

3 Sampling and analytical methods

3.1 Sampling strategy

Detailed sampling of a cross-section of the Huanghe was carried out on the 17th of July, 2016, during the flood season (Figure S2). Samples were collected along five depth profiles near the Luokou hydrological station (36.75ºN, 117.02ºE), 250 km upstream from the river mouth (Figure 1). This sampling strategy allows for accessing the full range of suspended sediment particle size (Bouchez et al., 2014). The cross-section is 200-meters wide at the surface and 4

meters deep at most (Figure 1; YRCC, 2016). As in previous studies, we used a home-made, 10-liter, point-sediment horizontal Niskin-type sampler attached to a current velocity meter, to collect river water samples and measure the water velocity simultaneously. Subsequently, two water samples were collected at the surface near the right bank in May and June 2017 before the flooding season, to retrieve fine suspended particulate matter. For each sample, approximately 30 liters of river water were collected and were then filtered through pre-weighed 0.22-µm porosity cellulose acetate membrane filters within 24 hours. After rinsing the filters with filtered water, all sediment samples were transferred into centrifuge tubes and freeze-dried before weighing and analysis. A bed sediment (BS) sample was collected on an exposed, recently flooded sediment bar of the riverbed.

3.2 Physical and geochemical analysis

Apart from a 50-mg aliquot of SPM samples preserved for particle size analysis, samples were finely ground using an agate mortar and pestle prior to chemical and isotopic analyses. The particle size distribution of the unground aliquots was measured using a Laser Diffraction Particle Size Analyzer (Beckman Coulter LS-12 320) at the École Normale Supérieure (ENS), Paris, France. Before analysis, unground SPM aliquots were dispersed in deionized water and then in sodium hexametaphosphate in an ultrasonic bath. For each sample, we measured three replicates and report the average median particle size (D50, µm) with an uncertainty better than 2% (Table 1). The chemical composition of SPM samples was measured on ground aliquots at the Centre de Recherches Pétrographiques et Géochimiques (CRPG), Vandoeuvre-lès-Nancy, France, using inductively coupled plasma atomic emission spectroscopy (ICP-OES) for major elements with typical uncertainties of 3% (Carignan et al., 2001).

For particulate organic carbon content (POC%, wt.), stable carbon isotope $\delta^{13}C$ (in ‰$_{VPDB}$, *i.e.*, in ‰ relative to Vienna Pee Dee Belemnite) and radiocarbon isotope $\Delta^{14}C$ (expressed as fraction modern, Fm), ground homogenized samples were fumigated using 12M HCl fumes in a closed Teflon tank at 60 °C for 48 hours to remove the carbonate fraction, and were then dried under vacuum prior to analysis. Total nitrogen content (TN%, wt.) was measured on non-acidified samples (Komada et al., 2008). Triplicate analysis on POC% and $\delta^{13}C$ of POC (acidified aliquots) as well as TN% (non-acidified aliquots) were carried out on an Organic Elemental Analyzer (OEA) coupled with Isotope Ratio Mass Spectrometry (IRMS, Thermo Scientific Flash 2000) under continuous flow mode at Géosciences Paris Saclay (GEOPS), Orsay, France. Subjected to the blank subtraction by linearity test, two international standards including USGS-40 and IAEA-600 as well as an internal standard (GG-IPG) were used to build linear regression equations to calibrate the elemental and isotopic values for both carbon and nitrogen. Uncertainties on POC%, $\delta^{13}C$, and TN%, based on replicate measurements (1σ, n=3), are lower than 0.02%, 0.06‰, and 0.02‰, respectively. The ^{14}C activity of POC was measured on a new compact accelerator mass spectrometry (AMS), *ECHo*MICADAS (Hatté et al., 2023), using a gas ion source interface system (GIS) at the Laboratoire des Sciences du Climat et de l'Environnement (LSCE), Gif-sur-Yvette, France, with an absolute uncertainty of max ±0.5%. Aside from the gas bottles of prepared blank PhA and standard NIST OX II which are permanently connected to the GIS and, used for normalization and corrections for fractionation and background, international standards including IAEA-C5, IAEA-C7, IAEA-C8, and blank PhA were prepared in different sizes (10 to 100's µg C) to match the amount of OC found in the sediment samples.

3.3 POC source apportionment

To quantify the contribution and associated uncertainties of various sources to POC transported in the Huanghe, a Bayesian Markov Chain Monte Carlo (MCMC) based on a three-end member (Appendix A) mixing scheme was adopted. This approach considers the variability on each end member contribution, assuming this variability can be represented by a normal distribution. Prior information is assumed to be unknown. We computed the posterior distribution of the Bayesian formulation using the MCMC method, facilitated by the *rjags* package (https://cran.r-project.org/web/packages/rjags/index.html, Andersson et al., 2015), all computations were performed in the R environment (http://www.r-project.org/). To ensure reliable simulation, the model was run with 5,000,000 iterations, using a burn-in of 1000 steps, and a data thinning of 100 for each sample. The mixing model was constructed on the dual stable and radioactive isotope of the riverine POC pool (δ^{13}C and Δ^{14}C) and of the three potential source pools (section 5.2) by the following equations:

$$\text{Isotope\_ratio}_{\text{sample}} = \sum_{\text{source}} (f_{\text{source}} * \text{Isotope\_ratio}_{\text{source}})$$

$$\sum_{\text{source}} f_{\text{source}} = 1$$

where Isotope_ratio$_{\text{sample}}$ is either the δ^{13}C or Δ^{14}C value of the sample, Isotope_ratio$_{\text{source}}$ is either the δ^{13}C or Δ^{14}C value of different possible sources of POC and f_{source} the relative contribution of each source of POC.

3.4 Depth-integrated fluxes

Instantaneous depth-integrated fluxes of SPM and POC sources were calculated for the cross-section using a method developed by Bouchez et al. (2011a, b). This method is based on the systematic variation of SPM concentration in the water column (Figure 2) applying a Rouse-based model (Rouse, 1937). We first constructed a bathymetric profile of the river cross-section based on the depth information collected in the field and then modeled the velocity distribution across the transect (Figure 1b) through fits of the so-called "law of the wall" to water velocity measured at the location of each sample within the cross-section using a current meter. Afterward, the concentration of total SPM and various particle size fractions could be estimated by applying the so-called Rouse model (Rouse, 1937) to each particle size fraction separately (Bouchez et al., 2011a), resulting in a map of the particle size distribution in the river cross-section (Figure S3). The aluminum to silicon ratio (Al/Si mass ratio) is inversely related to the particle size of river SPM in the Ganges-Brahmaputra, the Amazon, and the Mackenzie Rivers (Galy et al., 2007; Bouchez et al., 2014; Hilton et al., 2015). Such a linear relationship between D50 and Al/Si was also observed in our dataset, allowing for computing the spatial distribution of POC content in the cross-section, based on the linear relationship between POC and Al/Si (Figure 3). Finally, combining modeled water velocity, SPM concentration, and POC distribution we calculated a depth-integrated, instantaneous POC flux for the whole river channel (Figure S3, detail in supplementary material).

4 Results

We report the first isotopic dataset of POC samples collected along several depth profiles distributed over a cross-section of the Huanghe (Table 1). SPM concentrations range from 679 to 2,459 mg/L (avg. $1,286 \pm 572$ mg/L, reported with average value with one standard deviation, herein after) and show an obvious increase from the surface to the bottom and from the right bank to the left bank (Figure 1b and 2a). The surface SPM concentration (*i.e.*, samples collected 0.5 m below the surface) decreases laterally as the water column deepens. The range of measured Huanghe SPM D50*, i.e.* the median particle size (19.5-86.0 µm, Figure 2b) agrees with that (16.6-120.1 µm) of SPM collected at Lijin during the same flooding season by Moodie et al. (2022). In each depth profile, SPM is consistently coarsening with depth as revealed by the evolution of grain size parameters such as D10, D50, and D90 (Table 1, Figure 2 and Figure S4). The finest SPM is transported on the right bank and at the surface, while the coarsest SPM is found at the bottom of the middle profile (sample JB 2-3). Two types of depth profiles can be distinguished at Luokou based on particle size distributions (Figure S4) and the relationship between D50 and water depth (Figure 2b). On the one hand, the JB 1 and JB 4 profiles show a well-marked, bi-modal distribution of particle size (Figure S4) together with relatively low and consistent D50 (Figure 2b). On the other hand, the JB 2, JB 3, and JB 5 profiles show a more unimodal distribution of particle size (Figure S4) and a unique D50 - sampling depth relationship (Figure 2b). Interestingly, these two groups can also be distinguished in terms of relationships between POC% and $\delta^{13}C$ with water depth (Figures 2d and 2f). As expected, the Al/Si ratio is well-related to the particle size, and the ratios measured in the middle profile SPM samples (0.17 for JB 2-3 and 0.26 for JB 2-1) encompass the full range of Al/Si found in the whole cross-section (Figure 2c). The relatively low Al/Si ratios are comparable to that of the middle Huanghe (Qu et al., 2020) and other large turbid river systems such as the Ganges-Brahmaputra (Galy et al., 2008b), Salween, and Irrawaddy (Tipper et al., 2021).

SPM in the Huanghe is characterized by low TN and POC content (wt.%), ranging from 0.04% to 0.08% ($0.06 \pm 0.01\%$) and from 0.29% to 0.42% ($0.37 \pm 0.06\%$), respectively (Figure 2d; Table 1). POC content generally decreases from the surface to the river bed, with quantitative differences from one profile to another (Figure 2d). Notably, the JB 1 profile shows the highest POC% and TN%. In addition, the ratio of TN% to POC%: N/C_{org} increases with depth in the JB 1 profile (from top to bottom), while it decreases in the JB 2 and JB 3 profiles (Figure 2e). The $\delta^{13}C$ of POC varies over a narrow range from −26.55‰ to −25.75‰ ($−26.12 \pm 0.29‰$, Figure 2f) and becomes lighter with depth, showing that fine SPM has higher $\delta^{13}C$ than coarse SPM. These values are lower than those previously reported for other Huanghe sampling sites upstream: $−24.7 \pm 0.4‰$ at Toudaoguai, $−24.9 \pm 0.6‰$ at Longmen, and $−23.8 \pm 0.6‰$ at Lijin (Qu et al., 2020, Hu et al., 2015; Tao et al., 2015; Yu et al., 2019a; Ge et al., 2020). The radiocarbon activity of POC of the Huanghe at Luokou is relatively low (Figure 2g), with Fm ranging from 0.552 ($\Delta^{14}C = −453‰$; sample JB2-3) to 0.675 ($\Delta^{14}C = −331‰$; sample JB1-3), spanning from 3,160 to 4,780 ^{14}C yr, and the average value is 0.607 ± 0.038 ($\Delta^{14}C = −412‰$). This range of radiocarbon activity is consistent with published values for POC collected at the river surface downstream of Toudaoguai (Qu et al., 2020). All the POC radiocarbon activity data reported so far for the Huanghe are comparable to mean values for Arctic large rivers ($\Delta^{14}C = −397‰$, ca. 4,480 ^{14}C yrs, Ke et al., 2022), revealing the multimillennial-age nature of POC transported by the Huanghe. The elemental and isotopic signatures of the two fine SPM samples HH 17.05 and HH 17.06 (on average POC% = 1.07%, $\delta^{13}C$ = −25.67‰, F_m

 = 0.720; and Al/Si = 0.37) are significantly different from those of the depth profile samples (Table 1). The bed

248 sediment sample has a comparatively low POC% (0.21%), $\delta^{13}C$ (−27.35‰), F_m (0.099), and Al/Si ratio (0.17).
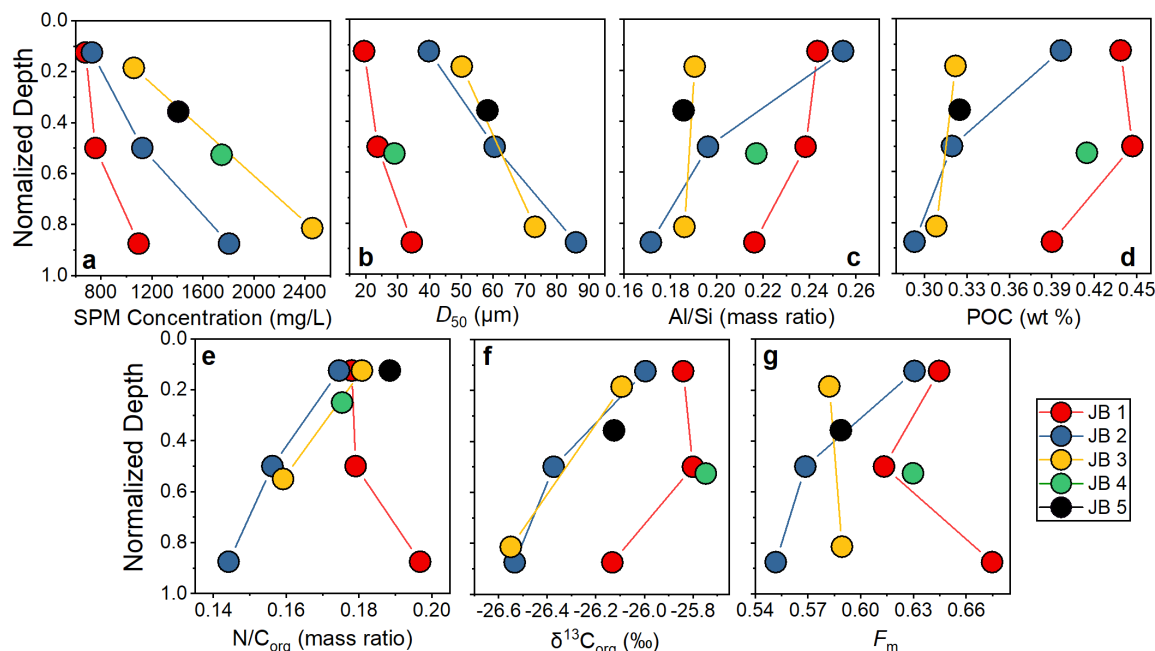
249
250 **Figure 2: Variation of physical and chemical parameters in the river cross-section, shown as a function of sampling depth**
251 **normalized to total depth of the water column at the location of the considered depth-profile, for the Luokou cross-section**
252 **on the Huanghe (June 16, 2017). (a) SPM concentration; (b) particle size distribution (shown as D50); (c) Al/Si mass ratio;**
253 **(d) POC content (weight %); (e) N/C$_{org}$ mass ratio; (f) stable carbon isotope ratio $\delta^{13}C_{org}$ (‰); (g) radiocarbon activity F_m.**

254 **Table 1: SPM characteristics and POC properties of the river-cross-section sampling.**

Sample ID	Type	Depth (m)	SPM mg/L	POC (%)	SD	$\delta^{13}C_{org}$ (‰)	SD	F_m	$\Delta^{14}C$ (‰)	SD	^{14}C age	TN (%)	N/C$_{org}$	Al/Si	D50 μm
JB 1-1	SPM	0.5	679	0.44	0.02	−25.84	0.03	0.645	−360	7	3527	0.078	0.178	0.243	19.5
JB 1-2	SPM	2	757	0.45	0.01	−25.80	0.06	0.613	−392	11	3929	0.080	0.179	0.238	23.7
JB 1-3	SPM	3.5	1095	0.39	0.01	−26.13	0.04	0.675	−331	7	3161	0.077	0.197	0.216	34.5
JB 2-1	SPM	0.5	730	0.40	0.03	−26.00	0.01	0.631	−374	7	3703	0.069	0.175	0.255	39.8
JB 2-2	SPM	2	1124	0.32	0.01	−26.37	0.06	0.569	−436	13	4537	0.050	0.156	0.196	60.4
JB 2-3	SPM	3.5	1806	0.29	0.01	−26.53	0.06	0.552	−453	38	4779	0.042	0.144	0.172	86.0
JB 3-1	SPM	0.5	1058	0.32	0.02	−26.09	0.03	0.582	−422	12	4346	0.058	0.181	0.190	50.1
JB 3-2	SPM	2.2	2459	0.31	0.02	−26.55	0.04	0.589	−415	11	4247	0.049	0.159	0.186	73.1
JB 4-1	SPM	1	1747	0.41	0.02	−25.75	0.06	0.630	−375	8	3714	0.073	0.175	0.217	29.0
JB 5-1	SPM	0.5	1406	0.32	0.01	−26.12	0.05	0.589	−416	11	4256	0.061	0.188	0.186	58.2
HH 17.05	SPM	0	83	0.92	0.00	−25.73	0.14	0.711	−295	19	2740	0.184	0.200	0.358	5.2
HH 17.06	SPM	0	54	1.21	0.01	−25.60	0.07	0.729	−277	25	2539	0.261	0.215	0.377	4.3
HH	BS			0.21	0.03	−27.35	0.05	0.099	−901	7	18539	0.019	0.087	0.175	44.4

5 Discussion

256 We observe significant heterogeneities of elemental and isotopic carbon composition as well as inorganic chemistry

257 over the studied river cross-section. The possible mechanisms behind these variations are assessed hereafter. Then,

258 sources of riverine POC are determined and quantified, confirming that erosion of the loess-paleosol sequence of the

259 CLP is a major source of aged and refractory biospheric OC to the Huanghe. Finally, we assess the POC load and its

260 variability over the transect profile, inferring the importance of the supply of POC from the river bottom in the
261 Huanghe.

5.1 Transportation mode of POC in the Huanghe

5.1.1 POC loading and its controls

264 The Huanghe is characterized by a high SPM load with relatively low POC% ($0.37 \pm 0.06\%$). In the Luokou cross-
265 section, POC content generally increases with decreasing particle size (Figure S5), with the two clay-sized ("HH")
266 samples showing the largest POC content (Table 1). Consistently, the Al/Si ratio of Huanghe sediments, which varies
267 as an inverse linear function of the median particle sizes D50 (R^2=0.72, p-value<0.05, Figure 3a), positively correlates
268 with POC% (R^2=0.81, p-value<0.05, Figure 3b), a pattern observed globally (Galy et al., 2008b; Bouchez et al., 2014;
269 Hilton et al., 2015; Repasch et al., 2021). This pattern is consistent with POC variability in the Huanghe reported for
270 manually separated size fractions of sediments (Yu et al., 2019b).
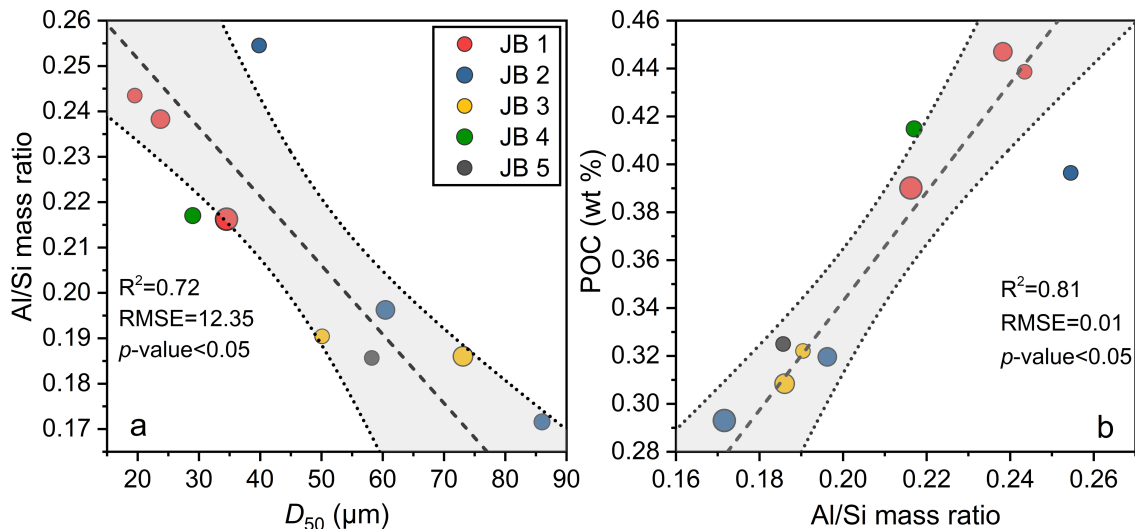
271
272 **Figure 3: Relationships between (a) particle size D50 and Al/Si mass ratio; (b) Al/Si mass ratio and POC content for the**
273 **Luokou cross-section on the Huanghe (July 17, 2016). Size of circles represents water depth of the corrresponding SPM.**
274 **The grey shade represents the 95% confidence area of the linear best-fit (black dashed line), the upper and lower bound**
275 **are marked by grey dotted lines.**

276 The first reason for the low POC content of Huanghe sediments is therefore their relatively low values of Al/Si
277 compared to other systems - a feature than can be related to the quartz-rich, OC-poor nature of the loess-paleosol
278 formations of the CLP (Jahn et al., 2021; Huang and Ren, 2006; He et al., 2006; Ning et al., 2006; Wang and Fu,
279 2016). However, Huanghe sediments are relatively poor in POC, even considering their low Al/Si, compared to other
280 rivers globally. To that effect, the so-called "POC loading" can be characterized by the slope described by sediment
281 data in an Al/Si-POC diagram (Galy et al., 2008b; Figure 4). For a given Al/Si ratio, the POC% in the Luokou cross-
282 section is similar to that of the middle Huanghe (Qu et al., 2020), indicating the relatively invariant transport mode of
283 POC between the middle and lower reaches. Previous studies have shown that the positive relationship between POC%
284 and Al/Si can be partially explained by OC adsorption onto the mineral surface (Curry et al., 2007; Galy et al., 2008b;
285 Blair and Aller, 2012; Bouchez et al., 2014; Qu et al., 2020). In the loess-paleosol deposits acting as a source of

286   sediments to the Huanghe, OC is mostly preserved and stabilized by forming organo-aggregates with kaolinite and

287   through adsorption onto iron oxides (Wang et al., 2013).

288   However, POC loading in the Huanghe is small compared to that of the Amazon (Bouchez et al., 2014), but similar

289   to that of the Ganges-Brahmaputra system (Galy et al., 2008b). While many factors could influence POC loading

290   across these catchments, we note that another similarity between the Huanghe and Ganges-Brahmaputra fluvial

291   systems is their millennial-aged OC_{bio} (Galy et al., 2007; Tao et al., 2016). This is in stark contrast with the Amazon,

292   where younger OC_{bio} ages have been reported (Bouchez et al., 2014). Given that younger OC_{bio} recently

293   photosynthesized in terrestrial or aquatic ecosystems can be readily oxidized within catchments (Mayorga et al., 2005),

294   the relatively low POC loading observed at the mouth of the Ganges-Brahmaputra and the Huanghe (Figure 4) could

295   be related to the predominance of refractory, aged OC_{bio} and OC_{petro} in those systems, while the Amazon sediments

296   would still contain significant amount of younger, more labile OC_{bio}.
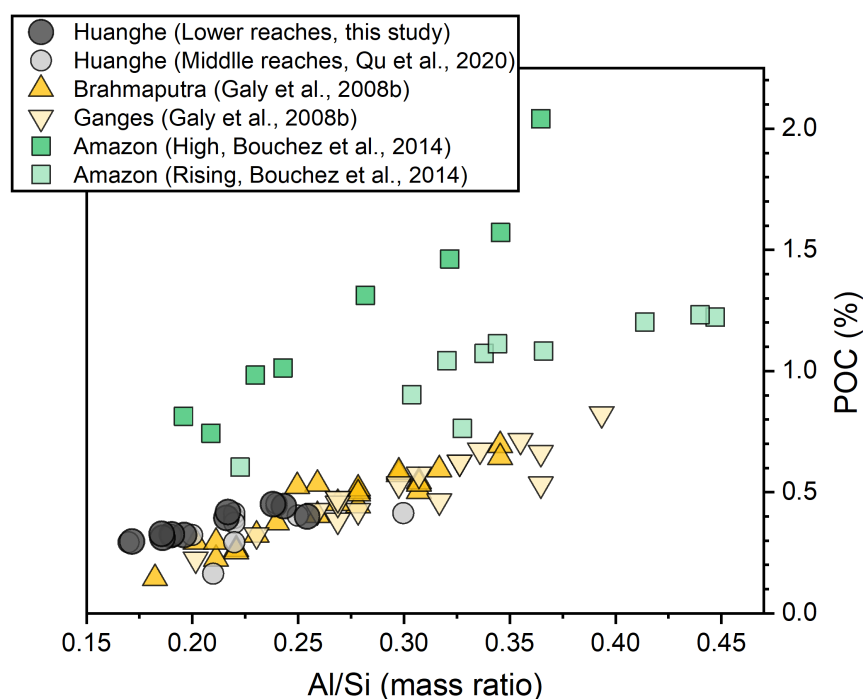
297
298   **Figure 4: "POC loading" of river SPM of large rivers. The POC loading is estimated from the slope of the relationship**
299   **between POC content and the Al/Si ratio of each fluvial system (Galy et al., 2008b). All SPM samples were collected along**
300   **depth profiles except for the middle Huanghe (Qu et al., 2020).**

301   In detail, and as explained in more detail below (**Section 5.1.2**) we also observe a significantly different POC loading

302   between the JB 1 and JB 2 depth profiles at the Luokou station (Figure 3). This difference in POC loading in the cross-

303   section of the Huanghe might indicate the delivery of recent OC_{bio}, specifically near the right bank (the closest to the

304   JB 1 profile) for the Luokou site, a scenario which is supported by the comparatively younger age of POC in profile

305   JB 1. Consistently with this interpretation, temporally variable POC loading at a given site has been reported for the

306   Amazon (Bouchez et al., 2014), where higher POC loading during the high-water stage compared to the rising water

307   stage has been attributed to the erosion of discrete organic debris from riverbanks.

308   Variable POC loading amongst large catchments has implications for evaluating the likelihood of POC preservation

309   in estuaries. The Ganges-Brahmaputra system delivers relatively old, refractory OC_{bio} to the Bengal Fan with an almost

310   complete burial efficiency (Galy et al., 2007). Given the observed similarity in POC loading and age, we can thus

311   expect a similar, efficient preservation for the Huanghe offshore depositional system. In addition to the low reactivity

312   of the POC transported by the Huanghe, the high sediment accumulation rates in the Huanghe coastal domain might

313   further inhibit OC oxidation (Blair and Aller, 2012). Consequently, the case of the Huanghe differs drastically from

314   that of the Amazon, where higher POC loading is observed, with a larger contribution of young, labile OC_{bio} either as

315   discrete organic matter or associated with mineral surfaces, leading to low POC burial efficiency in the ocean

316   (Bouchez et al., 2014; Blair and Aller, 2012).

5.1.2 Chemical heterogeneity within the transect

318   There is clear lateral and vertical variability of POC content and SPM inorganic chemistry across the Luokou cross-

319   section of the Huanghe. For each vertical depth profile, clay-rich fine particles are transported near the channel surface,

320   and quartz-rich coarse particles flow near the river bottom. Accordingly, the Al/Si ratio, POC content and POC

321   radiocarbon activity generally decrease with depth. Elemental (POC%) and isotopic POC signatures (^{13}C and ^{14}C) are

322   inversely related to the particle size (D50; Figure S5). These patterns are observed in other large fluvial systems, e.g.,

323   Ganges and Brahmaputra, Amazon and Mackenzie (Galy et al., 2008b; Bouchez et al., 2014, Hilton et al., 2015),

324   showing that hydrodynamic sorting is the primary control on suspended sediment OC content, segregating inorganic

325   and organic material according to particle size (Bouchez et al., 2011a, 2014).

326   At the Luokou sampling site, lateral variability at the channel surface shows that POC-rich fine particles are

327   preferentially transported near the right bank (Figure 2 and Figure S3). This pattern is validated by the Rouse model

328   provided in Text S1, the Rouse number (Z_R) is 0.137, 0.236, and 0.284 for JB-1, JB-2, and JB-3, respectively. In

329   essence, the Rouse number (Z_R) can reflect the balance between gravitation settling and upward turbulent diffusion.

330   Z_R is smaller near the right bank while larger near the left bank, showing heterogeneity across the transect. Larger

331   particles exhibit a faster settling velocity due to their increased weight, leading to a higher Z_R. On the other hand, the

332   lighter ones settle more slowly, resulting in Z_R approaching 0. This means that their concentration remains relatively

333   constant along a given depth profile. However, as depth increases and the concentration of larger particles grows, the

334   proportion of these finer particles in the overall sediment decreases (Bouchez et al., 2011a). The channel geometry

335   thus needs to be examined as a potential factor to produce such lateral heterogeneity, in particular the mechanisms of

336   bed sediment resuspension and bank erosion.

337   Resuspension of bed sediments is also a possible mechanism that could explain the lateral heterogeneity in POC

338   content in the study cross-section of the Huanghe. Indeed, scouring of channel bed sediment at high water flow may

339   also shift POC to more negative radiocarbon and stable isotope signatures. Our sample set collected in July 2016

340   during a flooding period (water flow velocity up to 2.1 m/s, Figure 1) supports this scenario. Indeed, the increase in

341   D50 of surface SPM samples from right to the left bank, that is with total channel depth decrease, is consistent with

342   coarse sediment resuspension from the bed. This is also supported by the Rouse model, where higher Zr in the shallow

343   water near the left bank indicates a greater likelihood of sediment settling to the bed, lower Zr suggests that there is

344   enhanced SPM supply from the riverbed. Such a scenario is also supported by the three-fold increase in SPM flux

observed from the upstream Huayuankou station to the downstream Lijin station in July 2016, despite a four-fold decrease in water discharge (Figure S2).

Bank erosion can be a significant mechanism for the delivery of sediments to river systems (Guo et al, 2007). Bank erosion at Luokou would make OC from the lower Huanghe alluvial plain a potential source of POC in the lower reaches of the Huanghe. Frequent inundation to the adjacent riparian zones in flooding seasons, surface runoff driven by storm events, and agriculture irrigation etc., can mobilize young soil OC and discrete organic matter debris (*e.g.,* plant-drived debris) to riverine POC (Hilton et al., 2011; Turowski et al., 2016). This mechanism provides a possible explanation for the opposite trends displayed by samples from the JB 1 and JB 2 profiles in the Fm *vs.* δ^{13}C space (Figure 5). The youngest POC was found at the bottom of the JB 1 profile (JB 1-3). Meanwhile, the JB 1 samples have comparatively higher N/C_{org} ratios and N%, consistent with the input of discrete plant-derived debris from the bank in addition to rock-derived detrital clastic material in the coarse fractions (> 32 μm, Yu et al., 2019b). The transport and entrainment of plant debris deep in the water column has been evidenced in many large river systems, such as the Amazon (Feng et al., 2016), the Ganges-Brahmaputra (Lee et al., 2019), the Mackenzie (Schwab et al., 2022), the Rio Bermejo River (Repasch et al., 2021). Such input would also provide an explanation for the higher POC loading of the JB 1 profile (**Section 5.1.1**).
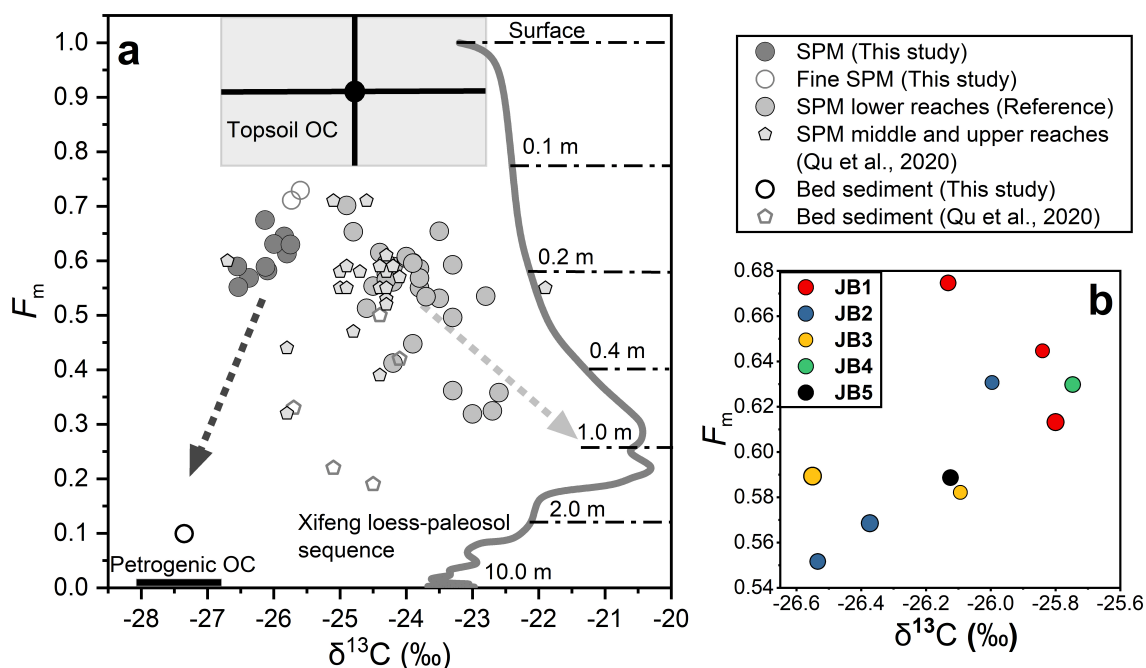
Figure 5: (a) ^{14}C activity (expressed as Fm) *vs.* δ^{13}C for a compilation of POC data collected over the 2011-2016 period in the lower Huanghe, including samples from this study and previous studies at Huayuankou, Lijin, and Kenli (Hu et al., 2015; Tao et al., 2015; Yu et al., 2019a; and Ge et al., 2020); SPM and bed sediment (BS) collected by Qu et al., 2020 at Toudaoguai (most downstream location of the upper reaches) and Longmen in the middle reaches (Table S1). The grey curve corresponds to $\delta^{13}C_{org}$ of the top 10 m of the Xifeng loess-paleosol (Ning et al., 2006), and the corresponding Fm was calculated from ^{10}Be-derived ages following 'Age = −8033*ln(Fm)'. The soil depth is marked above the dot-dash line (Zhou et al., 2010). Topsoil OC represents OC from the upper 10 cm of the loess-paleosol sequence with standard deviation marked

 with black lines. (b) ^{14}C activity (expressed as Fm) *vs.* δ^{13}C diagram for the Huanghe sediment samples collected in this
 study at the Luokou cross-section. Size of circles represents water depth of the corresponding SPM.

5.2 POC provenance in the Huanghe: the significance of loess-paleosol-derived OC

5.2.1 Physical erosion of the loess-paleosol sequence

Over decennial to centennial time scales, the POC export of the Huanghe is mainly controlled by erosion of the CLP. Throughout the Quaternary, the erosion rate in the Huanghe basin has been mainly driven by climate shifts until human activities started and profoundly impacted sediment fluxes in the mid-Holocene (He et al., 2006). The Huanghe has experienced a 90% decrease in annual sediment load since the 1950s (Wang et al., 2015), caused by weakened soil erosion to the CLP and sediment retention by dams (Wang et al., 2007; Ran et al., 2013; Wang and Fu et al., 2016; Li et al., 2022). To determine the contributions of the various terrestrial OC components to Huanghe POC, we compiled published POC carbon isotope data for sediments collected in the lower reaches from 2011 to 2016, after the Xiaolangdi Reservoir was operated (Figures 5 and 6). This dataset shows that the radiocarbon ages of Huanghe POC are considerably old (5,100 ± 1,700 ^{14}C yr, n=29), with a minor fraction of modern photosynthesized OC$_{bio}$ (Tao et al., 2015; Yu et al., 2019a, b). This relatively ^{14}C-depleted POC suggests the significant contribution of OC originated from deep soil horizons within the catchment. Given that loess is easily erodible and that there is widespread gully erosion in the catchment, more intensive erosion of the CLP can mobilize more soils as well as older OC from deep soil horizons to fluvial transport. Therefore, higher sediment load in the river can be characterized by radiocarbon-depleted POC. This is evidenced by the negative trend between ^{13}C and Fm of POC for sediment samples collected in the Huanghe over the 2011-2016 period (Figure 5a), suggesting that deep horizons of the loess-paleosol formations are a plausible source for the ^{14}C-depleted end member. Besides, the preferential erosion of bomb carbon affected, recently photosynthesized and possibly degraded OC$_{bio}$ from the overlying topsoils (< 10 cm) most likely contributes to riverine POC (Tao et al., 2015).

As such, variable contribution of aged and radiocarbon-free OC from deep horizons of loess-paleosol formations of the CLP should have a significant impact on the elemental and isotopic signature of POC in the lower Huanghe. Erosion of loess-paleosol can also explain the decreasing POC% with increasing SPM concentration at different sites of the main channel (Ran et al., 2013; Qu et al., 2020), the negative relationship between SPM concentration and corresponding POC Fm at Luokou (R^2=0.47, *p*-value<0.05, Figure 6), and the low POC loading of the Huanghe (section 5.1.1), as the deep horizons of the loess-paleosol sequences are OC-poor, and mostly host OC that is highly degraded and refractory (Liu et al., 2012; Wang et al., 2013; Cheng et al., 2020). However, the slight increase of POC δ^{13}C with increasing SPM concentration (R^2=0.26, *p*-value<0.05,) might indicate a significant supply of soil OC from loess-paleosol shallower depth, as inferred from the δ^{13}C variation within the Xifeng loess-paleosol sequence (Figure 5a).
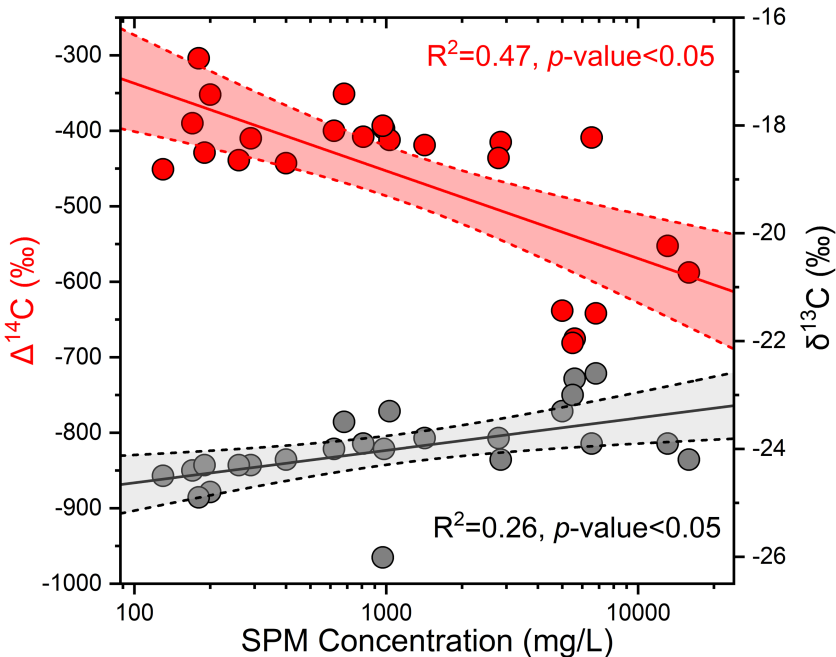
Figure 6: **^{14}C activity (expressed as Fm; red circles) and δ^{13}C (grey circles) of POC *vs*. SPM concentration for surface samples from the Huanghe collected from 2011 to 2016 (average SPM concentration of surface samples in this study and from Hu et al. (2015), Tao et al. (2015), Yu et al. (2019a), and Ge et al. (2020)). These paired dual carbon isotope data corresponds to the group 'SPM lower reaches' in Figure 5. Straight lines correspond to best-fit logarithmic curves, and shaded areas represent the 95% confidence interval.**

The N/C_{org} ratio provides additional evidence for the significant contribution of loess-paleosol material to Huanghe POC (Figure S6). Indeed, the N/C_{org} ratios of SPM collected in the lower reaches ranges from 0.10 to 0.23 (this study, Ran et al., 2013; Yu et al., 2019a), whereas topsoils of the CLP are characterized by N/C_{org} lower than 0.14 (Liu and Liu, 2017) and sedimentary rocks typically have very low N/C_{org} (Hilton et al., 2015). Soil OC input from the North China Plain is also unlikely given its N/C_{org} of 0.10-0.13 (Shi et al., 2017). Therefore, all these possible sources cannot explain the high N/C_{org} signatures of riverine SPM. In addition, the high turbidity of the Huanghe (> 600 mg/L) during the sampling season is likely to inhibit *in-situ* primary production (N/C_{org} > 0.13) (Zhang et al., 2013; Hu et al., 2015). As a result, only soil OC from deep loess-paleosol horizons appears as a plausible supplier to downstream Huanghe POC, given the high N/C_{org} ratios previously reported for various loess-paleosol sequences (Figure S6, Ning et al., 2006).

Geomorphic processes in the CLP region support the erosion of deep soil horizons. There, gully erosion is thought to be responsible for more than 80% of the total sediment yield in the CLP (He et al., 2006; Li et al., 2022). Gullies are densely distributed and cover about 42% of the total area of the CLP and up to 60% in hilly regions (Huang and Ren, 2006; He et al., 2006). Nowadays, the well-developed gully geomorphic system of the CLP is characterized by gullies with a depth of about 10 m on average and represents the most active vertical and regressive erosion of loess (Huang and Ren, 2006). This incision process erodes all types of unconsolidated materials, including the loess-paleosol sequence, underlaying red clays, and colluvial deposits in the form of creeps, falls, and slides in the watershed (Zhu, 2012). From 1925 to 1981, the erosion rate of the CLP was 6,318 t km^{-2} yr^{-1}, compared to 10,770 t km^{-2} yr^{-1} in the hilly and gully plateau (Li et al., 2022). While the CLP's erosion rate dropped to 3,476 t km^{-2} yr^{-1} between 1982 and

2016, the rate in the hilly and gully plateau remained significantly high at 6,146.5 t km^{-2} yr^{-1} (Li et al., 2022). All these observations suggest that gully erosion can strongly impact the composition of riverine POC. As gully erosion is sensitive to climate change and anthropogenic activities, soil dynamics in the Huanghe basin have been altered since the mid-Holocene (He et al., 2006; Li et al., 2022). Notably, the strengthening of the East Asian Monsoon in coming decades (Li et al., 2022; Xue et al., 2023) could potentially enhance this process. However, in recent years, soil and water conservation and environmental rehabilitation campaigns (Wang et al., 2007) largely contributed to the reduction of SPM export by the Huanghe with a transfer to the estuary of 10.6 Mt in 2016, which is one order of magnitude lower than the annual sediment flux measured in 2013 (172.8 Mt) and two orders or magnitude lower compared to the flux of the 1950s (*ca.* 1,340 Mt; Wang et al., 2015). This sediment load reduction is consistent with the weakened erosion rate observed in the CLP, such modifications should thus have drastically inhibited the OC mobilization from the CLP and the POC export by the Huanghe.

5.2.2 POC source determination and end member apportionment

Considering the SPM geochemistry and the basin characteristics, three terrestrial sources can be identified as necessary to form the composition of the Huanghe POC at the Luokou cross-section. As discussed in Section 5.2.1 and shown in Figure 5a, two of these sources are (a) topsoil-derived OC (OC$_{ts}$) and (b) OC from deeper horizons of the loess-paleosol sequence (OC$_{lps}$) excluding topsoil. In addition, at the Luokou cross-section, bed OC shows lower Fm and δ^{13}C values compared to that of SPM, suggesting a significant contribution of (c) rock-derived OC from erosion in the middle reaches (OC$_{petro}$).

We adopted a Bayesian Monte-Carlo model to reconstruct source apportionment based on the mass balance of carbon isotopes (δ^{13}C and Δ^{14}C) of our three defined end members (section 3.3, Table. 2, Appendix A). Modeling results are shown in Figure 7 as relative contributions (Figure 7a) and weight percentage (Figure 7b) of OC$_{ts}$, OC$_{lps}$, and OC$_{petro}$ (Table S2). The contribution of OC$_{petro}$ to total Huanghe POC at Luokou varies between 21% and 33% in the cross-section, which is higher than the contribution calculated for in the two fine SPM samples (17% on average) and much smaller than for the bed sediment sample (78 ± 10%). The inferred OC$_{petro}$ concentration in the sediment is remarkably uniform in the cross-section, representing 0.10 ± 0.01% of SPM (Figure 7b). This result is consistent with the OC contents of midstream sedimentary rocks at 0.09 ± 0.08% (Qu et al., 2020). In addition, these findings imply that OC$_{petro}$ concentration does not depend on particle size and confirm previous findings of OC$_{petro}$ being present in a range of clastic particles or as discrete particles (Galy et al., 2008a; Bouchez et al., 2014). In other words, the rock-derived OC has a relatively invariant contribution with depth (Galy et al., 2008a; Bouchez et al., 2014), meaning that biospheric OC exerts a first-order control on POC content and isotopic variations throughout the cross-section.

Table 2: Summary of δ^{13}C and Δ^{14}C of source end members for POC in the Huanghe.

End member	δ^{13}C	Δ^{14}C
OC$_{ts}$	−24.8 ± 1.9‰	−90 ± 130‰
OC$_{lps}$	−22.7 ± 1.0‰	−610 ± 390‰
OC$_{petro}$	−29.2 ± 0.9‰	-1000‰

At the study cross-section, OC$_{ts}$ and OC$_{lps}$ contribute 50%-60% and 17%-23% to the total POC, respectively (Figure 7a). The sum of these two components can be considered as OC$_{bio}$, which varies between 67% and 77%. The

458 corresponding OC$_{bio}$ content of sediment is quite variable, ranging from 0.20% (sample JB 2-3) to 0.34% (sample JB

459 1-1), and generally decreases from the river surface to the bottom. Given the rather invariant OC$_{petro}$ concentration in

460 the sediment, there are thus marked heterogeneities of POC provenance in the cross-section. For instance, POC

461 transported close to the right bank and in the finer SPM samples show a higher contribution from OC$_{bio}$. From the

462 knowledge of the relative contributions of OC$_{ts}$ and OC$_{lps}$ and their corresponding ^{14}C activity, the Fm values for the

463 bulk OC$_{bio}$ can be estimated based on mass balance. The modeled radiocarbon activity of OC$_{bio}$ is relatively

464 homogeneous with an average Δ^{14}C value of -178 ± 11‰ ($1{,}510 \pm 110$ ^{14}C yr) whereas a greater variance is observed

465 in the bulk ^{14}C content. In summary, our results support the first-order control of OC$_{bio}$ abundance on POC content

466 and age in the Huanghe.
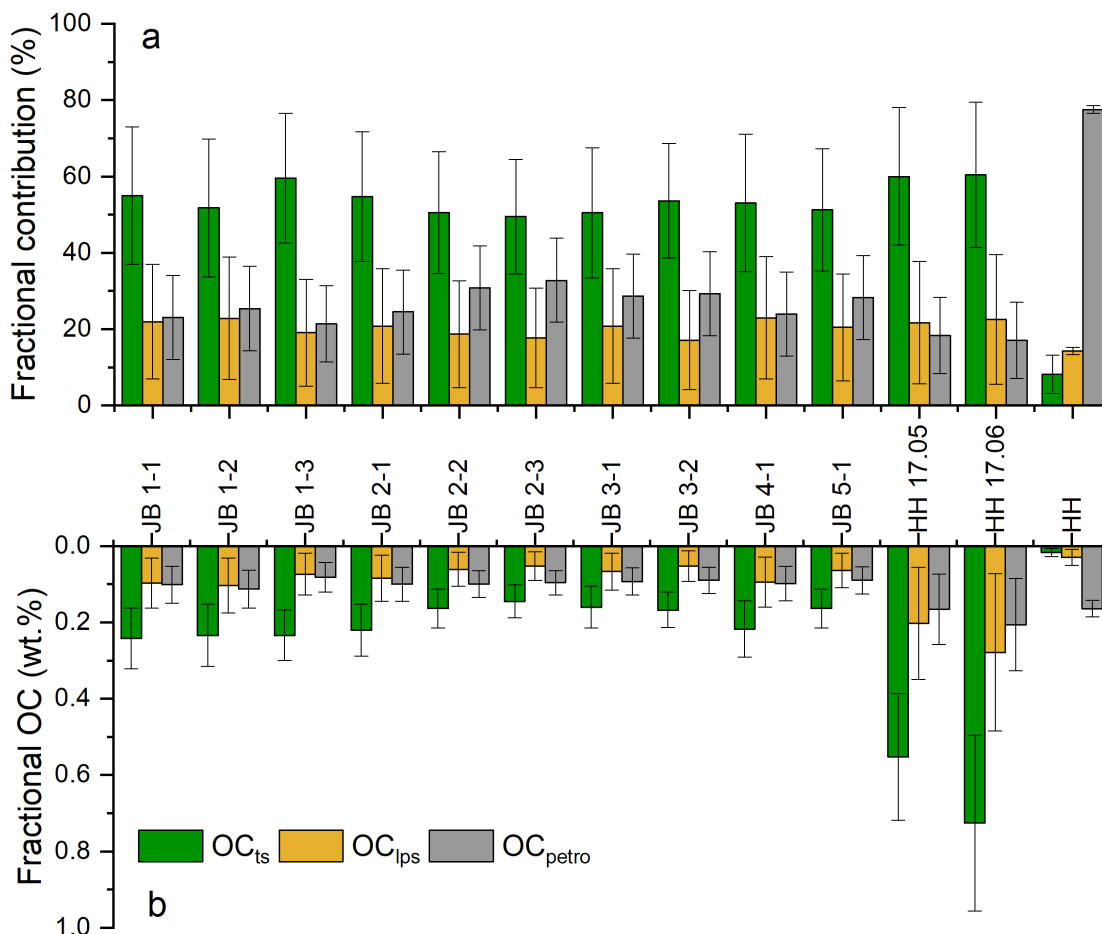
467
468 **Figure 7: (a) Relative contributions of the three different sources of Huanghe POC, (b) fractional OC weight percentage**
469 **Huanghe POC at the Luokou cross-section, as inferred from a mixing model. OC$_{ts}$ is the topsoil-derived OC, OC$_{lps}$**
470 **represents the loess-paleosol sequence OC excluding topsoil, and OC$_{petro}$ is the rock-derived OC eroded from the Huanghe**
471 **middle reaches.**

472 Applying the same mixing model to previously published Huanghe POC data (2011-2016, Table S1) shows (1)

473 dominance of the OC$_{bio}$ contribution to POC, (2) variable relative mixing proportions of OC$_{ts}$ and OC$_{lps}$; (3) a wide

474 range of ^{14}C age for OC$_{bio}$ (from 1,040 to 8,050 yr). In particular, OC$_{ts}$ and OC$_{lps}$ contributed 20%-30% and 46%-68%

475 to POC collected in 2013 (Hu et al., 2015), leading to 75-89% of OC$_{bio}$. Yu et al. (2019a) estimated that OC$_{bio}$

476 contributed 63%-81% to the lower Huanghe POC (2015-2016) using a different mixing model. Using their data in our

477 mixing model results in a slightly higher OC_{bio} contribution of 77%-87%, consisting of 39%-53% for OC_{ts} and 30%-
478 47% for OC_{lps}. The small difference in source contribution mainly results from the fact that old OC_{bio} from loess-
479 paleosol sequences was not considered in Yu et al. (2019a), and from the different isotopic signatures chosen for the
480 POC endmembers. However, both estimates ignore the possible presence of rock-derived OC in soils. In any case, our
481 results suggest that the Huanghe transports more OC_{bio}-derived POC than previously thought, with more aged, soil-
482 derived OC.

483 It is worth noticing that these calculations suggest that the OC_{lps} fraction in the Huanghe was significantly higher in
484 2013 than in 2016. As most Huanghe sediments are derived from the CLP, higher physical erosion in the CLP should
485 enhance supply of aged, refractory OC_{bio} to the river system. Consequently, the decrease in sediment supply from the
486 CLP initiated a few decades ago (Wang and Fu et al., 2016), which is likely to continue in the future, will probably
487 lead to the reduction of the contribution of OC_{lps} to total POC export from the Huanghe. This might have an impact
488 on the burial efficiency of riverine POC on the continental margins, as OC_{ts} is more labile than OC_{lps}, and thus more
489 prone to the remineralization process before burial. Moreover, decreasing erosion rate in the Huanghe basin will lead
490 to decreasing sediment accumulation rate in the estuary, which potentially favors the oxidation of all POC components
491 before burial (Blair and Aller, 2012). The time scale over which such effect could take place is yet unknown, as
492 anthropogenic intervention is the primary reason for the sediment yield reduction, through afforestation and soil and
493 water conservation measures in the CLP and reservoir operation in the middle reaches of the Huanghe. However, it is
494 plausible that in response to decreased terrestrial physical erosion on the Loess Plateau over at least decadal timescales,
495 an increased proportion of Huanghe POC will be oxidized before burial in the ocean, thereby leading to a weakened
496 preservation efficiency for the terrestrial eroded POC.

5.3 POC export by the Huanghe

498 In the Huanghe, POC content varies both vertically and laterally throughout the cross-section (Figure 2). This spatial
499 variability of both physical and chemical SPM characteristics must be considered when estimating integrated
500 instantaneous POC concentration and flux (Section 3.4).

501 We calculate that (Text S1) at the sampling time (July 2016), the Huanghe at Luokou transported 1,075 kg/s of SPM
502 for a water discharge of 731 m^3/s, such that the spatially-integrated SPM concentration over the cross section (SPM_{int})
503 was 1,472 mg/L, a value relatively close to the straightforward average concentration of our 10 samples (1,286 mg/L).
504 The Luokou gauging station records a monthly SPM load of 1,826 kg/s in July 2016, and the daily average SPM load
505 of 1,096 kg/s for a daily average water discharge of 643 m^3/s on the 16th and 17th of July 2016 (method: three water
506 samples collected at 0.5 m below the channel surface across the transect profile, data available at
507 http://www.yrcc.gov.cn). Even though the latter estimate neglects the vertical heterogeneity within this relatively
508 shallow river (< 5.0 m), estimates give similar results.

509 We further obtain an instantaneous POC flux of 3.69 kg/s, corresponding to a cross-section integrated average POC
510 content (POC_{int}%) of 0.34% when dividing this instantaneous POC flux by the instantaneous SPM load. Given the
511 relatively homogenous distribution of OC_{petro}, the instantaneous flux of OC_{petro} was calculated by multiplying the
512 average OC_{petro} content by the instantaneous cross-section integrated SPM flux, yielding 1.07 ± 0.11 kg/s. The

instantaneous OC_{bio} flux was then calculated by subtracting the instantaneous flux of OC_{petro} from the instantaneous POC flux, yielding 2.61 ± 0.26 kg/s. Assuming that our SPM samples are representative in terms of POC content exported in July 2016, and taking the SPM flux of the gauging station for July, then the estimated fluxes of POC, OC_{bio}, and OC_{petro} for the flood period of July 2016 are 6.1, 4.3, and 1.8 kg/s, respectively. Taking POC_{int} content for estimating the annual POC flux yields a value of 1.1 kg/s consisting of 0.8 and 0.3 kg/s for OC_{bio} and OC_{petro} fluxes, respectively. Note that these numbers are lower-bound estimates because POC content in Huanghe SPM collected during flood periods is generally the lowest (Ran et al., 2013). Taking the highest POC content 0.75% reported in the lower Huanghe in 2016 (Yu et al., 2019a), the estimated annual POC flux is 2.4 kg/s.

The above numbers present a sharp decrease compared to the estimated POC and OC_{bio} fluxes transported by the Huanghe over the period 2008 to 2013. Galy et al. (2015) estimated an OC_{petro} flux of 1.9 kg/s and an OC_{bio} flux of 11.4 kg/s from 2008 to 2012 (SPM flux: 3,655 kg/s, YRCC 2016), while Tao et al. (2018) reported an OC_{petro} flux of 5.8 kg/s and a similar OC_{bio} flux of 12.6 kg/s from June 2012 to May 2013 (SPM flux: 5,723 kg/s, YRCC 2016).

We first note that previous estimates of POC flux in the Huanghe might be biased as these estimates neglect the variability over the cross-section (*e.g.,* Hu et al., 2015; Ran et al., 2013; Tao et al., 2015), SPM samples analyzed so far for the Huanghe were generally collected within the first 0.5 m below the surface, meaning that previous POC estimates did not consider the observed vertical and lateral POC heterogeneities and have thus misestimated POC sources and fluxes. Those estimates were calculated by multiplying an individual surface POC content by the corresponding monthly or weekly suspended sediment load, as provided by hydrological stations. Such estimates can be problematic because POC content in SPM generally decreases from top to bottom (Figure 2), resulting in biased surface-based estimates of fluxes (Bouchez et al., 2014). Using our cross-section data, we can estimate the bias in POC flux estimates when a single sample is used for such flux estimates, by multiplying depth-integrated sediment flux by the POC content of each sample. Such calculation shows different POC fluxes ranging from −15% to +30% compared to the depth-integrated estimate, which is mostly influenced by the variable POC content. Considering SPM collected at the channel surface, POC flux estimates using samples JB 1-1 and JB 2-1 are 28% and 15% higher, respectively, and are 6% and 5% lower using samples JB 3-1 and JB 5-1, respectively, than the depth-integrated estimate. This simple sensitivity analysis shows that channel surface sampling of SPM alone does not necessarily result in an overestimation of POC flux because of lateral heterogeneity, even though the POC content of SPM is generally higher at the surface than at the bottom (Figure 2). As a consequence, and although accurate estimation of POC fluxes requires grain-size variations to be accounted for, the corresponding bias cannot explain the large difference between our estimates of Huanghe POC export for the year 2016 and previous estimates for preceding years. The SPM flux is 336 kg/s in 2016 and 762 kg/s over the period 2014 to 2016, which is one order of magnitude lower than values reported from 2008 to 2013 (YRCC 2016). The dramatic decrease in sediment load of the Huanghe (Wang and Fu et al., 2016) has most likely exerted a first-order control on the reduction in POC export from the Huanghe river system, and will probably continue to do so in the near future.

In the lower Huanghe, the POC content is very low and has small variance among different size fractions (Get et al., 2020), such that the POC flux is controlled by the SPM flux. In particular, it is worth noting that the Huanghe displays strong density stratification effects compared to other rivers (Moodie et al., 2022), with near-bed flow dominating the

550 transport of SPM. In order to appraise how spatial and temporal variability in SPM flux could influence POC export,
551 "local" POC loads can be calculated throughout the cross-section using the local water velocity, SPM concentration,
552 and POC content (Figure 8). In general, in the lower Huanghe more POC is transported near the riverbed and above
553 shallower bathymetry on the left side of the channel (except for profile JB 5). For instance, there is a nearly two-fold
554 increase in POC export from the surface to the bottom for the JB 2 and JB 3 profiles. The maximum local bulk POC
555 export (sample JB 3-2), OC_{bio} (sample JB 3-2), and OC_{petro} (sample JB 4-1) are over 6 times higher than the
556 corresponding minimum values (sample JB 5-1). This spatial pattern of POC load is almost the reverse of the POC%
557 variation over the cross-section, again stressing the importance of sediment river dynamics in POC delivery. From
558 these considerations, it could be anticipated that during the low-water season, when water velocity is slower, near-
559 bottom Huanghe SPM is deposited on the channel bed, withdrawing a significant fraction of the POC export, as shown
560 in other large rivers (Ke et al., 2022). This topic should be further examined in future research, in order to
561 systematically investigate the stratification of sediment and associated OC transport dynamics in lowland and high-
562 turbidity fluvial systems.
563
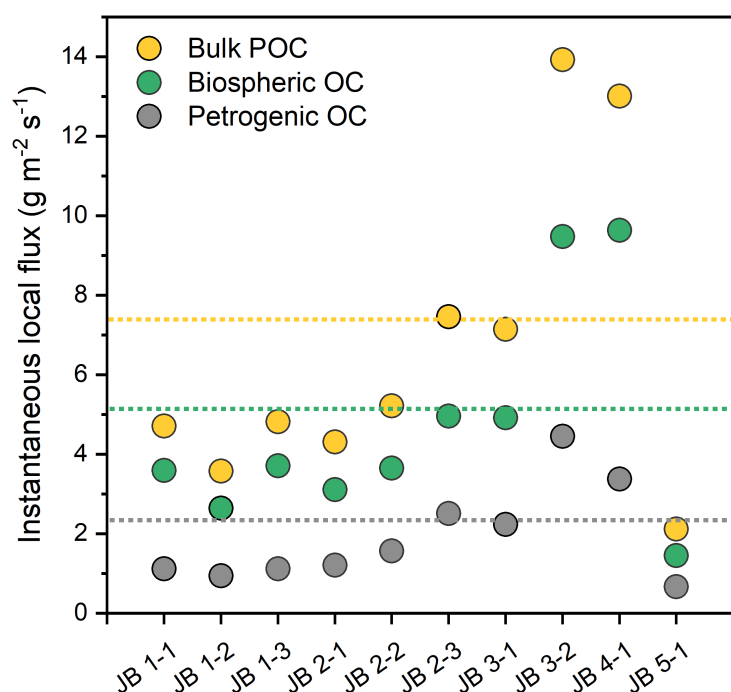
564
565 **Figure 8: Estimates of instantaneous "local" fluxes of Huanghe bulk POC, OC_{bio} and OC_{petro}, calculated for each sample of**
566 **the Luokou cross-section. The three dotted lines marked in orange, green, and grey represent the corresponding**
567 **instantaneous, cross-section integrated fluxes.**

568 Interestingly, anthropogenic activities may have antagonistic effects on POC export. Deforestation, agriculture, and
569 mining have considerably enhanced the sediment yield from the CLP since the mid-Holocene (He et al., 2006) while
570 the construction of large dams, soil and water conservation measures, and afforestation has considerably reduced the
571 sediment yield since the 1950s (Wang and Fu et al., 2016; Wang et al., 2007; Syvitski et al., 2005). Yet the Huanghe
572 exports substantial OC_{bio} and OC_{petro} with a significantly higher burial efficiency (~42% on average; Sun et al., 2018)
573 than other large fluvial systems entering passive continental margins, such as the Changjiang, Amazon, and

574 Mississippi (Blair and Aller, 2012). It is reported that aged soil OC is nearly fully preserved in continental margins

575 and that OC$_{petro}$ has a *ca.* 70% burial efficiency (Tao et al., 2016). However, the contribution of the Huanghe OC burial

576 to the global C sink is likely to be lower in the future as the consequence of 1) sharp decrease in SPM and POC export

577 due to weakened physical erosion in the CLP; 2) reduced sediment accumulation rate favoring OC remineralization

578 in estuaries (Blair and Aller, 2012; Walling and Fan, 2003; Milliman and Farnsworth, 2011; Galy et al., 2015).

579 6 Conclusions

580 In this contribution, we present the first detailed study of particulate organic carbon (POC) over a complete river cross-

581 section of the Huanghe, providing new perspectives on the transport mode, source, and instantaneous fluxes of POC

582 in this highly turbid large river.

583 At the scale of a cross-section, physical and chemical properties of SPM are heterogeneous both vertically and

584 laterally, a feature that is mainly controlled by bathymetry and hydrodynamic sorting. Resuspension of bed sediment

585 and local erosion of the right bank together impact the suspended POC composition at the sampled location. This

586 spatial heterogeneity shows that near-bottom SPM plays a dominant role in the delivery of OC$_{bio}$ (topsoil and deep

587 soil OC combined) and OC$_{petro}$. Despite a relatively shallow river channel (< 5.0 m) and narrow width (< 200 m), we

588 show how the heterogeneity of POC transport over a cross-section needs to be considered in constraining POC

589 transport mode and estimating POC fluxes.

590 Despite its millennial age, POC in the Huanghe is dominated by OC$_{bio}$ with a contribution of from 67% to 79%. OC$_{petro}$

591 content in SPM is relatively homogeneous (0.08% - 0.11%) over the cross-section, indicating that the variability in

592 bulk POC age is mainly controlled by the variability in OC$_{bio}$ content, especially in the finest SPM fraction. OC$_{bio}$ ages

593 deduced from the application of a mixing model to previously published data (record period 2011-2016) are highly

594 variable, ranging from 1,040 to 8,050 ^{14}C yr. We interpret this feature as resulting from the erosion of deep horizons

595 by gully systems in the loess-paleosol sequences containing ^{14}C-dead OC$_{bio}$. Enhanced erosion of deep loess-paleosol

596 horizons mobilizes aged and refractory OC to the ocean, with high burial efficiency on the passive margin. The erosion

597 of loess-paleosol horizons is thus an efficient process of CO_2 burial. However, the construction of large dams has

598 drastically affected the sediment load of the Huanghe system and retains substantial quantities of sediments that were

599 previously exported to the ocean. Future work is needed to further quantify how these anthropogenic modifications

600 alter POC composition and transport, by conducting comprehensive cross-section sampling campaigns over extended

601 time series upstream and downstream from dams.

602 **Appendix A**

603 Fluvial POC delivered in the Huanghe POC could originate from three terrestrial sources (Table. 2). As topsoil

604 typically contains recently photosynthesized OC$_{bio}$, we used a δ^{13}C value of −24.8 ± 1.9‰ (n=166) according to the

605 subsurface soil OC values measured across the Huanghe basin (Rao et al., 2017). Over the sampled cross-section, the

606 depleted ^{13}C values indicate the dominant and almost exclusive input of C3 plant-derived material to the Huanghe

607 POC in the lower reaches. Based on [14]C (Liu et al., 2012) and [10]Be (Zhou et al., 2010) dating of < 10 cm-deep soil

horizons in the Huanghe Basin, the average age of topsoil was chosen as being younger than 2,000 yr (*i.e.*, $\Delta^{14}C >$ −220‰). As the topsoil end member includes modern biospheric material ($\Delta^{14}C$ around 40‰, Hua et al., 2013), we assigned a $\Delta^{14}C$ value of −90 ± 130‰ (F_m = 0.91 ± 0.13) to this endmember. This range also includes the range of $\Delta^{14}C$ values of pre-aged soil OC indicated by the long-chain n-$C_{24+26+28}$ alkanols of the Huanghe POC reported by Tao et al. (2015) and Yu et al. (2019a). Their results show consistent POC $\Delta^{14}C$ values in the lower reaches of −204 ± 20‰ (F_m = 0.80 ± 0.03, n=7) from June 2015 to May 2016 and −219 ± 33‰ (F_m = 0.79 ± 0.04, n=4) at Kenli and of −198±15‰ (F_m = 0.81 ± 0.02, n=6) from June 2015 to April 2016 at Huayuankou.

The second end member should be characterized by aged and refractory OC from the loess-paleosol sequence excluding topsoil (upper 10 m) of the CLP. Radiocarbon dating has an upper age limit of around 50,000 yr, age above which F_m is equal to 0. However, radiocarbon-free OC spanning from 50,000 to 100,000 yr must still be considered as OC_{bio} in the long-term carbon cycle. Here, we name this ignored OC as the "dormant" OC, without which the OC_{bio} (*i.e.*, less than 100,000 yr old) would be underestimated to some extent because the radiocarbon-free OC would be misinterpreted as having a petrogenic origin. To consider this "dormant" OC, a $\delta^{13}C$ values of −22.7 ± 1.0‰ and a $\Delta^{14}C$ values of −610 ± 390‰ (F_m, 0.39 ± 0.39) were adopted based on an average of values over the whole loess-paleosol sequence. Although radiocarbon-free (*i.e.*, older than 100,000 yr) OC overlaps with this endmember, such old soil organic carbon is probably not mobilized as modern gully erosion mainly concerns the upper 10 m of the loess-paleosol sequences, where soil OC_{bio} is assumed to be significantly younger comparatively (Figure 5).

Rock-derived OC from the QTP and the CLP, as well as kerogen from oil-gas fields from the Ordos Basin, were all considered to be possible contributors to the OC_{petro} endmember. The $\delta^{13}C$ of OC_{petro} greatly varies between the QTP (−21.2 ± 1.2‰, n=11, Liu et al., 2007) and the CLP (−26.8 ± 0.5‰, n=8, Qu et al., 2020). However, most of the sediments eroded from the QTP are not transferred to the lower reaches as they remain trapped in the CLP and the western Mu Us desert (Nie et al., 2015; Licht et al., 2016; Pan et al., 2016). In addition, the construction of large dams in the upper reaches has considerably reduced the transfer of solid materials downstream (Wang et al., 2007). Therefore, rock-derived OC inherited from the denudation of the QTP region is not further considered. Kerogen from the oil-gas fields of the Ordos Basin in the CLP region (Figure 1) has $\delta^{13}C$ values of −29.2 ± 0.9‰ (n=10, Guo et al., 2014). Taking these constraints together, we consider a $\delta^{13}C$ value of −28.1 ± 1.5‰ for the OC_{petro} end member, and a $\Delta^{14}C$ value of −1000‰ (F_m = 0) by definition.

Key Points

- Bank erosion in lower Huanghe provides recent organic carbon to fluvial transport, altering the particulate organic carbon transport over a river channel cross-section;
- Erosion of deep soil horizons of the loess-paleosol sequence contributes radiocarbon-dead organic carbon from the biosphere to the Huanghe;
- Channel-bottom transport in the Huanghe is the primary process of exporting fluvial particulate organic carbon to the estuary.

Data availability

All datasets are included in the paper and the supplementary materials.

Author contributions

DC, JB, CQ, and YK conceptualized the study. DC, JB, YK, MM, and BC determined the methodology. HC and JC collected the sediment samples. YK, MM, and AN assisted with elemental and isotopic carbon analysis. DC and CQ supervised the work. KY performed data analysis and wrote the original draft, and all authors contributed to the review and editing of the paper.

Competing interests

We declare there is no competing interest.

Acknowledgments

We thank Yulong Liu and Shengliu Yuan for their help during sampling and filtering. We also thank François Thil and Nadine Tissenerat for invaluable help when running the ECHoMICADAS, and Pierre Barré for use of the Beckman Coulter's LS 13 320 for paticle size analysis at École normale supérieure.

Financial support

This study was financially supported by the Agence Nationale de la Recherche (ANR) SEDIMAN (Grant ANR-15-CE01-0012), the National Natural Science Foundation of China (NSFC), grants 41561134017, 41625012, and the China Scholarship Council (CSC) to Yutian Ke (No.201706180008).

References

Andersson, A., Deng, J., Du, K., Zheng, M., Yan, C., Sköld, M., and Gustafsson, Ö.: Regionally-Varying Combustion Sources of the January 2013 Severe Haze Events over Eastern China, Environ. Sci. Technol., 49, 2038–2043, https://doi.org/10.1021/es503855e, 2015.

Baronas, J. J., Stevenson, E. I., Hackney, C. R., Darby, S. E., Bickle, M. J., Hilton, R. G., Larkin, C. S., Parsons, D. R., Myo Khaing, A., and Tipper, E. T.: Integrating Suspended Sediment Flux in Large Alluvial River Channels: Application of a Synoptic Rouse-Based Model to the Irrawaddy and Salween Rivers, Journal of Geophysical Research: Earth Surface, 125, https://doi.org/10.1029/2020jf005554, 2020.

Bianchi, T. S.: The role of terrestrially derived organic carbon in the coastal ocean: A changing paradigm and the priming effect, Proceedings of the National Academy of Sciences, 108, 19473–19481, https://doi.org/10.1073/pnas.1017982108, 2011.

Bird, A., Stevens, T., Rittner, M., Vermeesch, P., Carter, A., Andò, S., Garzanti, E., Lu, H., Nie, J., Zeng, L., Zhang, H., and Xu, Z.: Quaternary dust source variation across the Chinese Loess Plateau, Palaeogeography, Palaeoclimatology, Palaeoecology, 435, 254–264, https://doi.org/10.1016/j.palaeo.2015.06.024, 2015.

Blair, N. E. and Aller, R. C.: The Fate of Terrestrial Organic Carbon in the Marine Environment, Annual Review of Marine Science, 4, 401–423, https://doi.org/10.1146/annurev-marine-120709-142717, 2012.

675   Blair, N. E., Leithold, E. L., Brackley, H., Trustrum, N., Page, M., and Childress, L.: Terrestrial sources and export of
676   particulate organic carbon in the Waipaoa sedimentary system: Problems, progress and processes, Marine Geology,
677   270, 108–118, https://doi.org/10.1016/j.margeo.2009.10.016, 2010.

678   Bouchez, J., Galy, V., Hilton, R. G., Gaillardet, J., Moreira-Turcq, P., Pérez, M. A., France-Lanord, C., and Maurice,
679   L.: Source, transport and fluxes of Amazon River particulate organic carbon: Insights from river sediment depth-
680   profiles, Geochimica et Cosmochimica Acta, 133, 280–298, https://doi.org/10.1016/j.gca.2014.02.032, 2014.

681   Bouchez, J., Gaillardet, J., France-Lanord, C., Maurice, L., and Dutra-Maia, P.: Grain size control of river suspended
682   sediment geochemistry: Clues from Amazon River depth profiles, Geochemistry, Geophysics, Geosystems, 12, n/a-
683   n/a, https://doi.org/10.1029/2010gc003380, 2011a.

684   Bouchez, J., Lupker, M., Gaillardet, J., France-Lanord, C., and Maurice, L.: How important is it to integrate riverine
685   suspended sediment chemical composition with depth? Clues from Amazon River depth-profiles, Geochimica et
686   Cosmochimica Acta, 75, 6955–6970, https://doi.org/10.1016/j.gca.2011.08.038, 2011.

687   Carignan, J., Hild, P., Mevelle, G., Morel, J., and Yeghicheyan, D.: Routine Analyses of Trace Elements in Geological
688   Samples using Flow Injection and Low Pressure On-Line Liquid Chromatography Coupled to ICP-MS: A Study of
689   Geochemical Reference Materials BR, DR-N, UB-N, AN-G and GH, Geostandards Newsletter, 25, 187–198,
690   https://doi.org/10.1111/j.1751-908X.2001.tb00595.x, 2001.

691   Cauwet, G. and Mackenzie, F. T.: Carbon inputs and distribution in estuaries of turbid rivers: the Yang Tze and Yellow
692   rivers (China), Marine Chemistry, 43, 235–246, https://doi.org/10.1016/0304-4203(93)90229-h, 1993.

693   Cheng, P., Burr, G. S., Zhou, W., Chen, N., Hou, Y., Du, H., Fu, Y., and Lu, X.: The deficiency of organic matter 14C
694   dating in Chinese Loess-paleosol sample, Quaternary Geochronology, 56, 101051,
695   https://doi.org/10.1016/j.quageo.2019.101051, 2020.

696   Curry, K. J., Bennett, R. H., Mayer, L. M., Curry, A., Abril, M., Biesiot, P. M., and Hulbert, M. H.: Direct visualization
697   of clay microfabric signatures driving organic matter preservation in fine-grained sediment, Geochimica et
698   Cosmochimica Acta, 71, 1709–1720, https://doi.org/10.1016/j.gca.2007.01.009, 2007.

699   Dellinger, M., Gaillardet, J., Bouchez, J., Calmels, D., Galy, V., Hilton, R. G., Louvat, P., and France-Lanord, C.:
700   Lithium isotopes in large rivers reveal the cannibalistic nature of modern continental weathering and erosion, Earth
701   and Planetary Science Letters, 401, 359–372, https://doi.org/10.1016/j.epsl.2014.05.061, 2014.

702   Feng, X., Feakins, S. J., Liu, Z., Ponton, C., Wang, R. Z., Karkabi, E., Galy, V., Berelson, W. M., Nottingham, A.
703   T., Meir, P., and West, A. J.: Source to sink: Evolution of lignin composition in the Madre de Dios River system
704   with connection to the Amazon basin and offshore, Journal of Geophysical Research: Biogeosciences, 121, 1316–
705   1338, https://doi.org/10.1002/2016JG003323, 2016.

706   Freymond, C. V., Lupker, M., Peterse, F., Haghipour, N., Wacker, L., Filip, F., Giosan, L., and Eglinton, T. I.:
707   Constraining Instantaneous Fluxes and Integrated Compositions of Fluvially Discharged Organic Matter, Geochem
708   Geophy Geosy, 19, 2453–2462, https://doi.org/10.1029/2018gc007539, 2018.

709   Gaillardet, J., Dupré, B., Louvat, P., and Allègre, C. J.: Global silicate weathering and CO2 consumption rates deduced
710   from the chemistry of large rivers, Chemical Geology, 159, 3–30, https://doi.org/10.1016/s0009-2541(99)00031-5,
711   1999.

712   Galy, V. and Eglinton, T.: Protracted storage of biospheric carbon in the Ganges–Brahmaputra basin, Nature Geosci,
713   4, 843–847, https://doi.org/10.1038/ngeo1293, 2011.

714   Galy, V., Beyssac, O., France-Lanord, C., and Eglinton, T.: Recycling of graphite during Himalayan erosion: a
715   geological stabilization of carbon in the crust, Science, 322, 943–5, https://doi.org/10.1126/science.1161408, 2008a.

716   Galy, V., France-Lanord, C., and Lartiges, B.: Loading and fate of particulate organic carbon from the Himalaya to
717   the Ganga–Brahmaputra delta, Geochimica et Cosmochimica Acta, 72, 1767–1787,
718   https://doi.org/10.1016/j.gca.2008.01.027, 2008b.

719   Galy, V., France-Lanord, C., Beyssac, O., Faure, P., Kudrass, H., and Palhol, F.: Efficient organic carbon burial in the
720   Bengal fan sustained by the Himalayan erosional system, Nature, 450, 407–10, https://doi.org/10.1038/nature06273,
721   2007.

722   Galy, V., Peucker-Ehrenbrink, B., and Eglinton, T.: Global carbon export from the terrestrial biosphere controlled by
723   erosion, Nature, 521, 204–7, https://doi.org/10.1038/nature14400, 2015..

724   Garzanti, E., Andò, S., France-Lanord, C., Vezzoli, G., Censi, P., Galy, V., and Najman, Y.: Mineralogical and
725   chemical variability of fluvial sediments: 1. Bedload sand (Ganga–Brahmaputra, Bangladesh), Earth and Planetary
726   Science Letters, 299, 368–381, https://doi.org/10.1016/j.epsl.2010.09.017, 2010.

727   Garcia, M.: Sedimentation Engineering, American Society of Civil Engineers, (pp. 21-163)
728   https://doi.org/10.1061/9780784408148, 2008.

Ge, T., Xue, Y., Jiang, X., Zou, L., and Wang, X.: Sources and radiocarbon ages of organic carbon in different grain size fractions of Yellow River-transported particles and coastal sediments, Chemical Geology, 534, 119452, https://doi.org/10.1016/j.chemgeo.2019.119452, 2020.

Gu, Z., Duan, X., Shi, Y., Li, Y., and Pan, X.: Spatiotemporal variation in vegetation coverage and its response to climatic factors in the Red River Basin, China, Ecological Indicators, 93, 54–64, https://doi.org/10.1016/j.ecolind.2018.04.033, 2018.

Guo, H., Jia, W., Peng, P., Lei, Y., Luo, X., Cheng, M., Wang, X., Zhang, L., and Jiang, C.: The composition and its impact on the methane sorption of lacustrine shales from the Upper Triassic Yanchang Formation, Ordos Basin, China, Marine and Petroleum Geology, 57, 509–520, https://doi.org/10.1016/j.marpetgeo.2014.05.010, 2014.

Guo, K., Zou, T., Jiang, D., Tang, C., and Zhang, H.: Variability of Yellow River turbid plume detected with satellite remote sensing during water-sediment regulation, Continental Shelf Research, 135, 74–85, https://doi.org/10.1016/j.csr.2017.01.017, 2017.

Guo, L., Ping, C.-L., and Macdonald, R. W.: Mobilization pathways of organic carbon from permafrost to arctic rivers in a changing climate, Geophysical Research Letters, 34, https://doi.org/10.1029/2007GL030689, 2007.

Guo, Z. T., Ruddiman, W. F., Hao, Q. Z., Wu, H. B., Qiao, Y. S., Zhu, R. X., Peng, S. Z., Wei, J. J., Yuan, B. Y., and Liu, T. S.: Onset of Asian desertification by 22 Myr ago inferred from loess deposits in China, Nature, 416, 159–163, https://doi.org/10.1038/416159a, 2002.

Hatté, C., Arnold, M., Dapoigny, A., Daux, V., Delibrias, G., Boisgueheneuc, D. D., Fontugne, M., Gauthier, C., Guillier, M.-T., Jacob, J., Jaudon, M., Kaltnecker, É., Labeyrie, J., Noury, C., Paterne, M., Pierre, M., Phouybanhdyt, B., Poupeau, J.-J., Tannau, J.-F., Thil, F., Tisnérat-Laborde, N., and Valladas, H.: Radiocarbon dating on ECHOMICADAS, LSCE, Gif-Sur-Yvette, France: new and updated chemical procedures, Radiocarbon, 1–16, https://doi.org/10.1017/RDC.2023.46, 2023.

He, X., Zhou, J., Zhang, X., and Tang, K.: Soil erosion response to climatic change and human activity during the Quaternary on the Loess Plateau, China, Reg Environ Change, 6, 62–70, https://doi.org/10.1007/s10113-005-0004-7, 2006.

Hemingway, J. D., Hilton, R. G., Hovius, N., Eglinton, T. I., Haghipour, N., Wacker, L., Chen, M. C., and Galy, V. V.: Microbial oxidation of lithospheric organic carbon in rapidly eroding tropical mountain soils, Science, 360, 209–212, https://doi.org/10.1126/science.aao6463, 2018.

Hemingway, J. D., Rothman, D. H., Grant, K. E., Rosengard, S. Z., Eglinton, T. I., Derry, L. A., and Galy, V. V.: Mineral protection regulates long-term global preservation of natural organic carbon, Nature, 570, 228–231, https://doi.org/10.1038/s41586-019-1280-6, 2019.

Hilton, R. G., Gaillardet, J., Calmels, D., and Birck, J.-L.: Geological respiration of a mountain belt revealed by the trace element rhenium, Earth and Planetary Science Letters, 403, 27–36, https://doi.org/10.1016/j.epsl.2014.06.021, 2014.

Hilton, R. G., Galy, A., Hovius, N., Horng, M.-J., and Chen, H.: Efficient transport of fossil organic carbon to the ocean by steep mountain rivers: An orogenic carbon sequestration mechanism, Geology, 39, 71–74, https://doi.org/10.1130/g31352.1, 2011.

Hilton, R. G., Galy, V., Gaillardet, J., Dellinger, M., Bryant, C., O'Regan, M., Grocke, D. R., Coxall, H., Bouchez, J., and Calmels, D.: Erosion of organic carbon in the Arctic as a geological carbon dioxide sink, Nature, 524, 84–7, https://doi.org/10.1038/nature14653, 2015.

Hu, B., Li, J., Bi, N., Wang, H., Wei, H., Zhao, J., Xie, L., Zou, L., Cui, R., Li, S., Liu, M., and Li, G.: Effect of human-controlled hydrological regime on the source, transport, and flux of particulate organic carbon from the lower Huanghe (Yellow River), Earth Surface Processes and Landforms, 40, 1029–1042, https://doi.org/10.1002/esp.3702, 2015.

Hua, Q., Barbetti, M., and Rakowski, A. Z.: Atmospheric Radiocarbon for the Period 1950–2010, Radiocarbon, 55, 2059–2072, https://doi.org/10.2458/azu_js_rc.v55i2.16177, 2013.

Huang, C. C., and Ren, Z: Fluvial erosion and the formation of gully systems over the Chinese Loess Plateau, WSEAS Transactions on Environment and Development, 2(2), 141-145, 2006.

Jahn, B., Gallet, S., and Han, J.: Geochemistry of the Xining, Xifeng and Jixian sections, Loess Plateau of China: eolian dust provenance and paleosol evolution during the last 140 ka, Chemical Geology, 178, 71–94, https://doi.org/10.1016/S0009-2541(00)00430-7, 2001.

Ke, Y., Calmels, D., Bouchez, J., and Quantin, C.: MOdern River archivEs of Particulate Organic Carbon: MOREPOC, Earth System Science Data Discussions, 1–19, https://doi.org/10.5194/essd-2022-161, 2022.

Keil, R. G., Mayer, L. M., Quay, P. D., Richey, J. E., and Hedges, J. I.: Loss of organic matter from riverine particles in deltas, Geochimica et Cosmochimica Acta, 61, 1507–1511, https://doi.org/10.1016/S0016-7037(97)00044-6, 1997.

784   Gen Li, X. T. W., Zhongfang Yang, Changping Mao, A. Joshua West, Junfeng Ji: Dam-triggered organic carbon
785   sequestration makes the Changjiang (Yangtze) river basin (China) a significant carbon sink, Journal of Geophysical
786   Research: Biogeosciences, 2015.
787   Li, P., Chen, J., Zhao, G., Holden, J., Liu, B., Chan, F. K. S., Hu, J., Wu, P., and Mu, X.: Determining the drivers and
788   rates of soil erosion on the Loess Plateau since 1901, Science of The Total Environment, 823, 153674,
789   https://doi.org/10.1016/j.scitotenv.2022.153674, 2022.
790   Licht, A., Pullen, A., Kapp, P., Abell, J., and Giesler, N.: Eolian cannibalism: Reworked loess and fluvial sediment as
791   the main sources of the Chinese Loess Plateau, GSA Bulletin, 128, 944–956, https://doi.org/10.1130/B31375.1, 2016.
792   Liu, G., Xu, W., Zhang, Q., & Xia, Z. : Holocene Soil Chronofunctions, Luochuan, Chinese Loess Plateau.
793   Radiometric Dating, 41, 2012.
794   Liu, J. and Liu, W.: Soil nitrogen isotopic composition of the Xifeng loess-paleosol sequence and its potential for use
795   as a paleoenvironmental proxy, Quaternary International, 440, 35–41, https://doi.org/10.1016/j.quaint.2016.04.018,
796   2017.
797   Liu, W., Yang, H., Ning, Y., and An, Z.: Contribution of inherent organic carbon to the bulk $\delta^{13}C$ signal in loess
798   deposits from the arid western Chinese Loess Plateau, Organic Geochemistry, 38, 1571–1579,
799   https://doi.org/10.1016/j.orggeochem.2007.05.004, 2007.
800   Ludwig, W., Probst, J.-L., and Kempe, S.: Predicting the oceanic input of organic carbon by continental erosion,
801   Global Biogeochemical Cycles, 10, 23–41, https://doi.org/10.1029/95gb02925, 1996.
802   Mayorga, E., Aufdenkampe, A. K., Masiello, C. A., Krusche, A. V., Hedges, J. I., Quay, P. D., Richey, J. E., and
803   Brown, T. A.: Young organic matter as a source of carbon dioxide outgassing from Amazonian rivers, Nature, 436,
804   538–41, https://doi.org/10.1038/nature03880, 2005.
805   Milliman, J. D. and Farnsworth, K. L.: River discharge to the coastal ocean: a global synthesis, Cambridge University
806   Press, 2011.
807   Milliman, J. D., Yun-Shan, Q., Mei-E, R., and Saito, Y.: Man's Influence on the Erosion and Transport of Sediment
808   by Asian Rivers: The Yellow River (Huanghe) Example, The Journal of Geology, 95, 751–762,
809   https://doi.org/10.1086/629175, 1987.
810   Moodie, A. J., Nittrouer, J. A., Ma, H., Carlson, B. N., Wang, Y., Lamb, M. P., and Parker, G.: Suspended Sediment-
811   Induced Stratification Inferred From Concentration and Velocity Profile Measurements in the Lower Yellow River,
812   China, Water Resources Research, 58, e2020WR027192, https://doi.org/10.1029/2020WR027192, 2022.
813   Ning, Y., Liu, W., and An, Z.: Variation of soil $\delta^{13}C$ values in Xifeng loess-paleosol sequence and its
814   paleoenvironmental implication, CHINESE SCI BULL, 51, 1350–1354, https://doi.org/10.1007/s11434-006-1350-7,
815   2006.
816   Pan, B., Pang, H., Gao, H., Garzanti, E., Zou, Y., Liu, X., Li, F., and Jia, Y.: Heavy-mineral analysis and provenance
817   of Yellow River sediments around the China Loess Plateau, Journal of Asian Earth Sciences, 127, 1–11,
818   https://doi.org/10.1016/j.jseaes.2016.06.006, 2016.
819   Qu, Y., Jin, Z., Wang, J., Wang, Y., Xiao, J., Gou, L.-F., Zhang, F., Liu, C.-Y., Gao, Y., Suarez, M. B., and Xu, X.:
820   The sources and seasonal fluxes of particulate organic carbon in the Yellow River, Earth Surface Processes and
821   Landforms, https://doi.org/10.1002/esp.4861, 2020.
822   Ran, L., Lu, X. X., and Xin, Z.: Erosion-induced massive organic carbon burial and carbon emission in the Yellow
823   River basin, China, Biogeosciences, 11, 945–959, https://doi.org/10.5194/bg-11-945-2014, 2014.
824   Ran, L., Lu, X. X., Sun, H., Han, J., Li, R., and Zhang, J.: Spatial and seasonal variability of organic carbon transport
825   in the Yellow River, China, Journal of Hydrology, 498, 76–88, https://doi.org/10.1016/j.jhydrol.2013.06.018, 2013.
826   Rao, Z., Guo, W., Cao, J., Shi, F., Jiang, H., and Li, C.: Relationship between the stable carbon isotopic composition
827   of modern plants and surface soils and climate: A global review, Earth-Science Reviews, 165, 110–119,
828   https://doi.org/10.1016/j.earscirev.2016.12.007, 2017.
829   Repasch, M., Scheingross, J. S., Hovius, N., Lupker, M., Wittmann, H., Haghipour, N., Gröcke, D. R., Orfeo, O.,
830   Eglinton, T. I., and Sachse, D.: Fluvial organic carbon cycling regulated by sediment transit time and mineral
831   protection, Nat. Geosci., 14, 842–848, https://doi.org/10.1038/s41561-021-00845-7, 2021.
832   Rouse, H.: Modern Conceptions of the Mechanics of Fluid Turbulence, Transactions of the American Society of Civil
833   Engineers, 102, 463–505, https://doi.org/10.1061/TACEAT.0004872, 1937.
834   Schwab, M. S., Hilton, R. G., Haghipour, N., Baronas, J. J., and Eglinton, T. I.: Vegetal Undercurrents—Obscured
835   Riverine Dynamics of Plant Debris, Journal of Geophysical Research: Biogeosciences, 127, e2021JG006726,
836   https://doi.org/10.1029/2021JG006726, 2022.
837   Shi, H. and Shao, M.: Soil and water loss from the Loess Plateau in China, Journal of Arid Environments, 45, 9–20,
838   https://doi.org/10.1006/jare.1999.0618, 2000.

839 Stevens, T., Carter, A., Watson, T. P., Vermeesch, P., Andò, S., Bird, A. F., Lu, H., Garzanti, E., Cottam, M. A., and
840 Sevastjanova, I.: Genetic linkage between the Yellow River, the Mu Us desert and the Chinese Loess Plateau,
841 Quaternary Science Reviews, 78, 355–368, https://doi.org/10.1016/j.quascirev.2012.11.032, 2013.

842 Sun, D., Tang, J., He, Y., Liao, W., and Sun, Y.: Sources, distributions, and burial efficiency of terrigenous organic
843 matter in surface sediments from the Yellow River mouth, northeast China, Organic Geochemistry, 118, 89–102,
844 https://doi.org/10.1016/j.orggeochem.2017.12.009, 2018.

845 Syvitski, J. P. M., Vörösmarty, C. J., Kettner, A. J., and Green, P.: Impact of Humans on the Flux of Terrestrial
846 Sediment to the Global Coastal Ocean, Science, 308, 376–380, https://doi.org/10.1126/science.1109454, 2005.

847 Tao, S., Eglinton, T. I., Montluçon, D. B., McIntyre, C., and Zhao, M.: Pre-aged soil organic carbon as a major
848 component of the Yellow River suspended load: Regional significance and global relevance, Earth and Planetary
849 Science Letters, 414, 77–86, https://doi.org/10.1016/j.epsl.2015.01.004, 2015.

850 Tao, S., Eglinton, T. I., Montluçon, D. B., McIntyre, C., and Zhao, M.: Diverse origins and pre-depositional histories
851 of organic matter in contemporary Chinese marginal sea sediments, Geochimica et Cosmochimica Acta, 191, 70–88,
852 https://doi.org/10.1016/j.gca.2016.07.019, 2016.

853 Tao, S., Eglinton, T. I., Zhang, L., Yi, Z., Montluçon, D. B., McIntyre, C., Yu, M., and Zhao, M.: Temporal variability
854 in composition and fluxes of Yellow River particulate organic matter, Limnology and Oceanography, 63, S119–S141,
855 https://doi.org/10.1002/lno.10727, 2018.

856 Turowski, J. M., Hilton, R. G., and Sparkes, R.: Decadal carbon discharge by a mountain stream is dominated by
857 coarse organic matter, Geology, 44, 27–30, 2016.

858 Walling, D. E. and Fang, D.: Recent trends in the suspended sediment loads of the world's rivers, Global and Planetary
859 Change, 39, 111–126, https://doi.org/10.1016/S0921-8181(03)00020-1, 2003.

860 Wang, C., Li, F., Shi, H., Jin, Z., Sun, X., Zhang, F., Wu, F., and Kan, S.: The significant role of inorganic matters in
861 preservation and stability of soil organic carbon in the Baoji and Luochuan loess/paleosol profiles, Central China,
862 CATENA, 109, 186–194, https://doi.org/10.1016/j.catena.2013.04.001, 2013.

863 Wang, G., Feng, X., Han, J., Zhou, L., Tan, W., and Su, F.: Paleovegetation reconstruction using δ^{13}C of Soil Organic
864 Matter, Biogeosciences, 5, 1325–1337, https://doi.org/10.5194/bg-5-1325-2008, 2008.

865 Wang, H., Bi, N., Saito, Y., Wang, Y., Sun, X., Zhang, J., and Yang, Z.: Recent changes in sediment delivery by the
866 Huanghe (Yellow River) to the sea: Causes and environmental implications in its estuary, Journal of Hydrology, 391,
867 302–313, https://doi.org/10.1016/j.jhydrol.2010.07.030, 2010.

868 Wang, H., Wu, X., Bi, N., Li, S., Yuan, P., Wang, A., Syvitski, J. P. M., Saito, Y., Yang, Z., Liu, S., and Nittrouer, J.:
869 Impacts of the dam-orientated water-sediment regulation scheme on the lower reaches and delta of the Yellow River
870 (Huanghe): A review, Global and Planetary Change, 157, 93–113, https://doi.org/10.1016/j.gloplacha.2017.08.005,
871 2017.

872 Wang, H., Yang, Z., Saito, Y., Liu, J. P., Sun, X., and Wang, Y.: Stepwise decreases of the Huanghe (Yellow River)
873 sediment load (1950–2005): Impacts of climate change and human activities, Global and Planetary Change, 57, 331–
874 354, https://doi.org/10.1016/j.gloplacha.2007.01.003, 2007.

875 Wang, S., Fu, B., Piao, S., Lü, Y., Ciais, P., Feng, X., and Wang, Y.: Reduced sediment transport in the Yellow River
876 due to anthropogenic changes, Nature Geosci, 9, 38–41, https://doi.org/10.1038/ngeo2602, 2016.

877 Wang, X., Xu, C., Druffel, E. M., Xue, Y., and Qi, Y.: Two black carbon pools transported by the Changjiang and
878 Huanghe Rivers in China, Global Biogeochemical Cycles, 2016.

879 Weiguo, L., Xiahong, F., Youfeng, N., Qingle, Z., Yunning, C., and Zhisheng, A. N.: δ^{13}C variation of C3 and C4
880 plants across an Asian monsoon rainfall gradient in arid northwestern China, Global Change Biology, 11, 1094–1100,
881 https://doi.org/10.1111/j.1365-2486.2005.00969.x, 2005.

882 Xiubin, H., Tang, K., and Zhang, X.: Soil Erosion Dynamics on the Chinese Loess Plateau in the Last 10,000 Years,
883 mred, 24, 342–347, https://doi.org/10.1659/0276-4741(2004)024[0342:SEDOTC]2.0.CO;2, 2004.

884 Xue, D., Lu, J., Leung, L. R., Teng, H., Song, F., Zhou, T., and Zhang, Y.: Robust projection of East Asian summer
885 monsoon rainfall based on dynamical modes of variability, Nat Commun, 14, 3856, https://doi.org/10.1038/s41467-
886 023-39460-y, 2023.

887 YRCC (Yellow River Conservation Committee): Annual Sediment Report for the Yellow River, 2016.

888 Yu, M., Eglinton, T. I., Haghipour, N., Montlucon, D. B., Wacker, L., Hou, P., Zhang, H., and Zhao, M.: Impacts of
889 Natural and Human-Induced Hydrological Variability on Particulate Organic Carbon Dynamics in the Yellow River,
890 Environ Sci Technol, 53, 1119–1129, https://doi.org/10.1021/acs.est.8b04705, 2019a.

891 Yu, M., Eglinton, T. I., Haghipour, N., Montluçon, D. B., Wacker, L., Wang, Z., Jin, G., and Zhao, M.: Molecular
892 isotopic insights into hydrodynamic controls on fluvial suspended particulate organic matter transport, Geochimica et
893 Cosmochimica Acta, 262, 78–91, https://doi.org/10.1016/j.gca.2019.07.040, 2019b.

894   Zhang, L. J., Wang, L., Cai, W. J., Liu, D. M., and Yu, Z. G.: Impact of human activities on organic carbon transport
895   in the Yellow River, Biogeosciences, 10, 2513–2524, https://doi.org/10.5194/bg-10-2513-2013, 2013.
896   Zhu, T. X.: Gully and tunnel erosion in the hilly Loess Plateau region, China, Geomorphology, 153–154, 144–155,
897   https://doi.org/10.1016/j.geomorph.2012.02.019, 2012.